Chapter 8

Sensor Placement Optimization of a Helicopter Main Rotor Blade

Chapter details

Chapter DOI:

https://doi.org/10.4322/978-65-86503-88-3.c08

Chapter suggested citation / reference style:

Pereira, João L. J., et al. (2022). "Sensor Placement Optimization of a Helicopter Main Rotor Blade". *In* Jorge, Ariosto B., et al. (Eds.) *Uncertainty Modeling: Fundamental Concepts and Models*, Vol. III, UnB, Brasilia, DF, Brazil, pp. 221–257. Book series in Discrete Models, Inverse Methods, & Uncertainty Modeling in Structural Integrity.

P.S.: DOI may be included at the end of citation, for completeness.

Book details

Book: Uncertainty Modeling: Fundamental Concepts and Models

Edited by: Jorge, Ariosto B., Anflor, Carla T. M., Gomes, Guilherme F., & Carneiro, Sergio H. S.

Volume III of Book Series in:

Discrete Models, Inverse Methods, & Uncertainty Modeling in Structural Integrity

Published by: UnB City: Brasilia, DF, Brazil Year: 2022

DOI: https://doi.org/10.4322/978-65-86503-88-3

Sensor Placement Optimization of a Helicopter Main Rotor Blade

João Luiz Junho Pereira[1*], Matheus Brendon Francisco[2], Ariosto Bretanha Jorge[3], and Guilherme Ferreira Gomes[4]

[1]Mechanical Engineering Institute, Federal University of Itajubá (UNIFEI), Itajubá, Brazil – joaoluizjp@unifei.edu.br mailto:joaoluizjp@unifei.edu.br
[2] Management and Production Engineering Institute, Federal University of Itajubá (UNIFEI), Itajubá, Brazil – matheus_brendon@unifei.edu.br
[3]Post-Graduate Program - Integrity of Engineering Materials, University of Brasilia, Brazil. E-mail: ariosto.b.jorge@gmail.com
[4]Mechanical Engineering Institute, Federal University of Itajubá (UNIFEI), Itajubá, Brazil – guilhermefergom@unifei.edu.br;

*Corresponding author

Abstract

This chapter describes the importance of one of the major areas within Structural Health Monitoring and Health and Usage Monitoring Systems: Sensor Placement Optimization (SPO). In this sense, the most important SPO metrics are presented and discussed with the reader. The methodological procedure of the optimization problem statement is also considered and discussed. he significance of rotary-wing aircraft, damages that can occur in the blade, works related to damage identification, modern methods and algorithms that have been used in this context, and a comprehensive SPO study for a helicopter main rotor blade will be presented. Finally, a new technique that considers the number of sensors as an objective associated with some of the main metrics used in SPO. The technique uses the Multi-objective Lichtenberg Algorithm and Feature Selection, an important area used in Data Mining.

Keywords: Structural Health Monitoring, Sensor Placement Optimization, Helicopter rotor blade.

1 Introduction

Helicopters have great importance due to its capabilities of travel speed (200-300 km/h) and maneuverability, which promotes movement along the shortest track and vertical takeoff (Khabarov & Komshin [2021]). These unique qualities make this aircraft efficient for urban transport of people, rescue in hard places, use on offshore oil rigs and military forces, among other applications.

Being a rotary-wing aircraft, or rotorcraft, its most important element is the main rotor blade (MRB), which is usually made of composite material. Due to the intense in-service conditions of aerodynamics, temperature variation, and accelerations, damage can be induced in these structures (Ahmad *et al*. [2020]). Some examples are: fracture of matrix, delamination (most important), fiber breakage, fiber waviness, creep deformation, etc. (VOICU *et al*. [2020]).

As a matter of fact, composite structures don´t give any clue till the collapse. It is necessary to have methodologies for the assessment, identification and prediction of damages in order to avoid catastrophic failures. Efficient systems, such as Structural Health Monitoring (SHM) or Health and Usage Monitoring Systems (HUMS), allow early identification of damage through non-destructive inspection and integrated sensors exploring vibration/modal measures. The method is based on the principle that a damaged in a structure changes natural frequencies, mode shapes, modal strain energy and damping ratios (Gomes *et al*. [2020]; Pereira *et al*. [2021]).

Then, it is possible to identify the damage using inverse modeling and computational intelligence analyzing the output vibration parameters of the system. The main data processing techniques used, nowadays, are meta-heuristics, neural networks, non-probabilistic methodologies, and time-series analyses. However, there is no methodology that is very effective for all problems. New technologies have been proposed and there is space for new ones (Burgos [2020]). There are not many works in the literature that have been dedicated to studying damage in MRB and most modeled the study using some direct method, that is, the problem is elaborated and their answers are directly analyzed.

In case of experimental studies, Cattarius & Inman [2000] induced punctual increase and decrease of mass and observed significant variations of natural frequencies in a real MRB. A fact also proved by Santos *et al*. [2013]. Ghoshal *et al*. [2001] tested different types of sensors and concludes that those linked to modal properties are the most reliable in damage identification. Kiddy & Pines [2001] used an experimental methodology to conclude that localized damage in low modal energy locations is difficult to detect. Santos *et al*. [2016] compared coordinate modal assurance criterion and modal strain energy method to detect damage on a full-size composite MRB. The authors concluded that the last method was more sensitive to the presence of damage.

Equally important, other authors used numerical modeling to carry out their related studies. Pawar & Ganguli [2005] studied the effect of matrix cracks in composite MRB using strain measurement and concludes that is possible to find the localization and density of a matrix cracks using this metric. The same authors extend the study to delaminations and fiber breakage, analyzing stiffness, natural frequencies, deflections, root forces, root moments and strains in forward flights (Pawar & Gangulli, [2007c]). The authors also concluded that modal data are appropriate for damage identification. In like manner, Ahmad *et al.* [2020] created a faithful MRB with contour conditions and forces identical to a flight situation to study the progressive failure. The authors found that failure starts from the root chord and tend toward the tip chord. Shahani & Mohammadi [2015] analyzed the fatigue life of a numerical blade using safe-life and damage tolerance approaches and concludes that the skin is the component that has the shortest lifetime.

The first works using SHM and inverse methods associated with finite element method (FEM) updating on MRB appeared at the beginning of the century. Pawar & Ganguli [2003] created a genetic fuzzy system to find the damage location and extent: a fuzzy system qualifies the changes in natural frequencies in four damage levels and the Genetic Algorithm (GA) optimizes its rule-base and membership functions. Despite being a qualitative damage identification and the authors have used a composite beam as a MRB, the methodology proved to be efficient. The same authors used the same strategy in two other studies: *i*) using displacements instead natural frequencies and residual life classes instead damage levels (Pawar & Gangulli, [2007]) and *ii*) changing the genetic fuzzy system by the Support Vector Machine (SVM) classifier, still using natural frequencies to find damage levels, having success even in noisy situations (Pawar & Gangulli, [2007b]). Reddy & Ganguli [2003] used artificial neural networks (ANN) with modal data generated by the FEM to identify MRB damage. The authors have success and concluded that is enough use the first 5 mode shapes.

Up to the present time, Gomes *et al.* [2020b] was the first to propose a methodology for identifying MRB damage that locate and quantify the damage severity. The authors proposed an inverse method using the FEM updating associated with the Bat Optimization Algorithm (BA) and uniformly distributed 10 sensors on the blade to measure displacements due to mode shapes.

As can be seen, none of them proposed a MRB Sensor Placement Optimization (SPO) methodology. Just like none of them either proposed a methodology using multi-objective meta-heuristics. At the same time, modern methodologies have been proposed for damage identification in other structures using: *i*) FEM updating, *ii*) frequency response function, *iii*) ground excitation, *iv*) signal processing, v) new machine learning algorithms, among others. The FEM updating is the most precise and have two ways: *i*) direct problem modeling, where a structural numerical model is made, and *ii*) inverse problem modeling, where the model is constantly evaluated by an optimization algorithm that minimizes an objective function composed by structural characteristics (Milad *et al*. [2019]; Assis & Gomes [2021]).

The SPO problem in structures can be complex, multi-modal, with multiple variables and even multiple objective functions. The complexity becomes even greater if there is interest in sensors number reduction. Therefore, the efficiency of the methodology and the quality of the answers strongly depend on the optimization algorithm used and meta-heuristics have proven to be the best.

Some important works using mono-objective meta-heuristics in SPO are: *i*) Genetic Algorithm (GA) (Gomes *et al*. [2019]), *ii*) Ant Colony Optimization (ACO) (Braun *et al*. [2015]; Mishra *et al*. [2019]), *iii*) Particle Swarm Optimization (PSO) (Chen & Yu [2018]; Kaveh & Maniat [2015]), *iv*) Firefly Algorithm (FA) (Pan *et al*. [2016]), *v*) Sunflower Optimization (SFO) (Gomes *et al*. [2019]), *vi*) BA (Zenzen *et al*. [2018]; Gomes *et al*. [2020b]), among others.

However, recent studies indicate that the use of multi-objective meta-heuristics, given their ability to evaluate several metrics at the same time, has found better results both in SPO and in damage identification (Alkayem *et al*. [2017]; Gomes *et al*. [2018], Zhou *et al*. [2021]). Furthermore, the fundamental principle of SHM is select the smallest number possible of measurement locations from a structure and represent the system with the highest possible accuracy, which are obviously conflicting objectives (Barthorpe & Worden [2009]; Pereira *et al*. [2021b]).

Even so, the studies found in SPO aims cost or energy minimization while the efficiency of data reading is improved: *i*) Ferentinos & Tsiligiridis [2007]: wireless sensors, *ii*) Lin *et al*. [2018]: three-dimensional truss structure, *iii*) Gomes *et al*. [2018]: The first using FIM and MSI at the same time, finding excellent results, i*v*) Cao *et al*. [2020]: proposed a method named distance coefficient-multi-objective information fusion algorithm (D-MOIF) and two objective functions based on other metrics. The author was the first to study SPO in a more complex structure, *v*) Zhou *et al.* [2021]: showed that the Multi-objective FA obtained better results than the NSGA-II, and *vi*) Colombo *et al*. [2022]: proposed a statistical methodology that evaluated the positioning of sensors together with the damage identification.

To the best author's knowledge, no works are found that consider the number of sensors as one of the objectives. In larger and more complex structures, as in a MRB, the need to develop multi-objective methodologies that select the smallest number of sensors that bring the maximum information about the structure is essential. The first study to do so was recently published and is the result of the Research Group in Computational Mechanics (GEMEC) at UNIFEI (Pereira *et al*. [2022b]**)**. The technique uses the Multi-objective Lichtenberg Algorithm and techniques employed in Feature Selection, an important area in Data Mining. The methodology applied as well as unpublished information will be presented in this chapter.

So, in this chapter will be introduced the importance of studying SPO in an MRB, discussing in detail the appearance of damage in it, how these damages influence its mechanical properties, how the problem of SPO is treated, including your main metrics and makes a case study of SPO considering a single objective, maximizing one of the main metrics, and considering these same metrics, but having the number of sensors as an objective in a multi-objective SPO.

2 Backgrounds

The concepts necessary for the development of this chapter are: *i*) types and characteristics of damages in MRB, *ii*) how modal data can help identify damage, *iii*) the main metrics used to interpret and analyze modal data, and *iv*) what is the Lichtenberg Algorithm meta-heuristic and its multi-objective version, not yet shown in this book series.

2.1 Damage in main helicopter rotor blade

Composite materials have distinctive qualities, such as low weight, high strength, remarkable stiffness related to its specific mass, and high capacity to withstand fatigue and corrosion. These reasons justify using them in the manufacture of MRB, which have in their constructions multiple constituents and a pronounced anisotropic behavior. However, they may have failure mechanisms. In addition to possible manufacturing defects, the helicopter in flight can present severe conditions of aerodynamics, temperature variation, and accelerations loads that contribute to emergence of damage (Ahmad *et al*. [2020]).

Small defects in blade fabrication, such as autoclave molding, resin transfer mold or resin film infusion, can progress severely when in operation. The main damages resulting from this are: non-uniformly positioned laminae, uneven distributed resin, missing or cut fibers, incomplete resin maturation, porosity or trapped air bubbles, signs of wear or scratches on the material, and fiber or weave undulation (Huo & Zhang [2012]).

In operation, overloads, environmental factors or impact with foreign objects can aggravate previous manufacturing defects or give rise to new damages. Some examples are: fracture of matrix, fiber breakage, debonding, delamination, fiber waviness, and creep deformation (Voicu *et al*. [2020]). A matrix crack develops between two or more parallel laminae and can propagate beyond them. Despite being a type of damage that does not present an immediate risk, it can be a starting mechanism for more serious ones. However, fiber breakage considerably reduces the Young´s modulus and the load bearing capacity of the material, what makes it a damage that requires more attention (Amafabia *et al*. [2017]).

Debonding occurs when the adhesive cannot bonds the surfaces which it is applied, which happens when external or environmental loads breakage chemical, physical, or mechanical links between the surface and adhesive. According to Voicu *et al*. [2020], material ageing, low speed impact or flaws in the development process can lead to this damage. Another damage that considerably reduces the strength of a composite material is the fiber waviness. This damage appears due to the local buckling of prepreg or wet hoop-wound filaments strand (Vinet & Gamby [2008]).

The most critical and important damage is delamination, which appears as the result of impact of foreign objects. This damage can lead the entire structure to failure, as the material strength is proportional with the degree of delamination (Latifi *et al*. [2015]). This damage is the loss of stiffness in the material due to spaces formed between the adjacent layers of a laminate and is the main source of cracks in composite structures (Pantano [2019]).

2.2 Damage monitoring using modal data

These damages cause structural degradation and change natural frequencies, mode shapes, modal strain energy and damping ratios in very particular ways. Then, it is possible to identify the damage using inverse modeling and computational intelligence analyzing the output modal parameters of the system.

The most used modal properties in damage identification are natural frequencies and mode shapes (Gomes *et al*., [2020]). Both have their advantages and drawbacks. According to Gopalakrishnan *et al*. [2011], natural frequencies have low sensitivity in determining damage location when compared to mode shapes. However, according to Worden & Friswell [2009], natural frequencies can be estimated very accurately (1% error) without a complete modal test. A single random excitation test can determine it through a basic spectral analysis. Still, according to Guan *et al*. [2017], it can be obtained using a single and random structural point.

According to Hearn & Testa [1991], the change of the *i*-th natural frequency after a change in the global stiffness matrix ΔK_N in a damaged structure is represented by Equation (1).

$$\Delta\omega_i{}^2 = \frac{(\in_N(\Phi_i))^T \Delta K_N (\in_N(\Phi_i))}{\Phi_i{}^T M \Phi_i} \quad (1)$$

where Φ_i defines the *i*-th mode shape, M is the mass matrix, and $\in_N(\Phi_i)$ is the strain vector calculated by the mode shape.

However, while the natural frequency is a property that considers the entire structure, mode shapes are able to provide local modal properties. For this reason, it has been the most used to identify localized damage. It has greater sensitivity to structural damage and provides detailed information about the extent and location of it (Pereira *et al.*, [2021]; Gomes *et al.* [2018]).

The mode shapes are the eigenvectors Φ and natural frequencies are the eigenvalues λ of the problem expressed in Equation (2). Both can be obtained solving this Equation.

$$\left[K - \lambda_i M\right]\Phi_i = 0 \quad (2)$$

where Φ_i is the eigenvector associated with the *i*-th mode shape, λ_i is the eigenvalue, M is the mass matrix, and K is the stiffness matrix, which is the most affected matrix when damage comes.

In delamination case, for example, the stiffness matrix is the only one affected and according to Pereira *et al.* [2021], the variation in the *i*-th mode shape is in Equation (3):

$$\Delta\Phi_i = \sum_{r=1, r\neq i}^{p} \frac{-\Phi_r^T \Delta K \Phi_i}{\lambda_r - \lambda_i} \quad (3)$$

where Φ_i is the eigenvector and λ_i the eigenvalue associated with the *i*-th mode shape, ΔK is the variation stiffness matrix, and λ_r the eigenvalue and Φ_r the eigenvector associated with the damaged structure.

Solving these equations for complex structures is not an easy task. However, advances in computing and FEM make it possible to obtain, both natural frequencies and mode shapes, for any type of structure and for any given excitation range in fast numerical simulations. Therefore, it is possible through the mode shapes to calculate the displacement of any point of this structure for each of the natural frequencies, due to the particular ways that each structure vibrates when excited near its natural frequencies. Figure 1 shows the mode shapes of a helicopter main rotor blade (MRB).

Using FEM, the variation of the global stiffness matrix is simplified as shown Equation (4). Many authors have used this equation to represent delaminations (PEREIRA *et al.* [2021]; GOMES *et al.*, [2020b]).

$$\Delta K = \sum_{k=1}^{N} \alpha_K K_K \quad (4)$$

where α is a scalar multiplier (between 0 and 1) that modifies the original K stiffness in the k element.

FEM is a powerful tool that allows finding the displacement at each node in each mode shape, however, it is unable to answer the following question: where and how many sensors should I place on a specific structure to obtain as much information as possible about how it vibrates? Note that the answer to this question not only allows identifying the sensing that provides the highest level of information about the structure, but also allows for a more accurate and efficient damage identification.

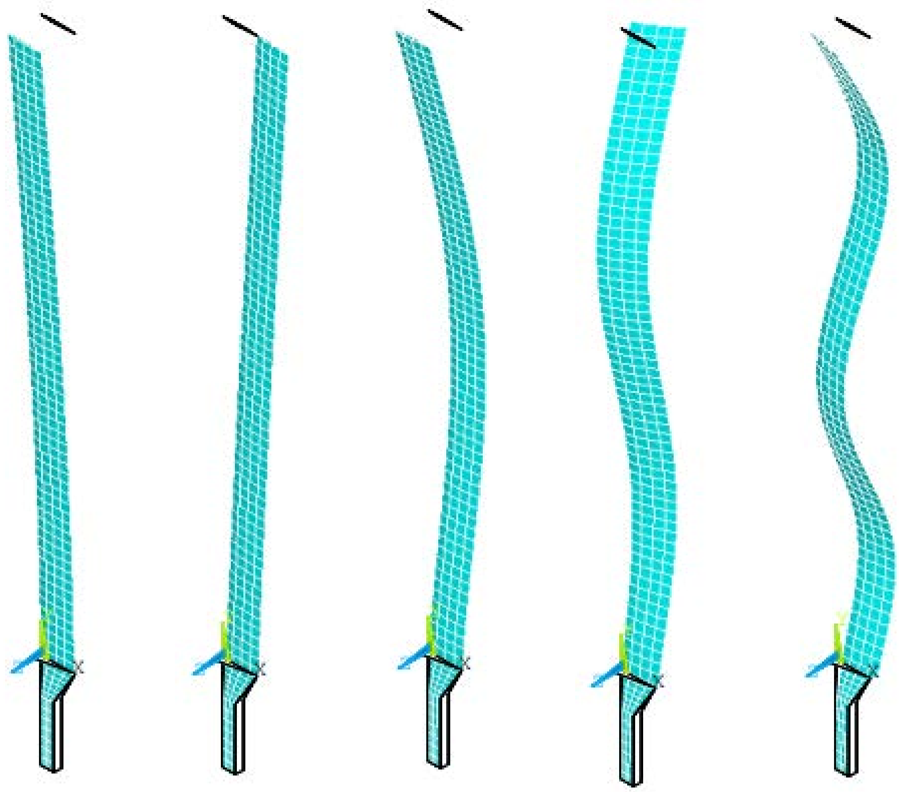

a) 1.1 Hz b)5.5 Hz c)6.7 Hz d)17.8 Hz e)32.5 Hz

Figure 1: First five MRB natural frequencies (adapted from Pereira *et al.* [2022b])

It is intuitive for the reader to imagine that the more sensors, the more information will be acquired and that is one of the biggest challenges of sensor positioning: a greater number of sensors means more weight, cost, processed data size, and changes to the modal properties of the structure as more mass, wiring, and other items are added to it. Therefore, it is shown that the acquisition of information and the number of sensors are conflicting objectives and from here arises an area within SHM called Sensor Placement Optimization (SPO).

Knowing that each point of a structure in a given mode shape is a point where a displacement can be measured and therefore a sensor can be installed, it is intended to identify which combinations of these sensors provide the greatest displacements and still use as few sensors as possible. To answer this question, several SPO metrics have been proposed, which although they approach these displacement measures in different ways, they all aim for the same answer.

2.3 Modal metrics in Structural Health Monitoring

This section presents the main SPO metrics used in recent years. From them, an objective function can be proposed so that, when optimized by an optimization algorithm, the set of sensors that delivers the most information is obtained. Some best known metrics are: Kinetic Energy (KE) (Heo *et al*. [1997]), Effective Independence (EfI) (Yang & Lu [2017]), Average Driving-Point Residue (ADPR) (Barthorpe & Worden [2009]), Eigenvalue Vector Product (EVP) (Barthorpe & Worden [2009]), Information Entropy (IE) (Yuen & Kuok [2015]), Fisher Information Matrix (FIM) (Benner *et al*. [2017]), and Modal Assurance Criterion (MAC) (Jin *et al*. [2015]).

The main component of all these metrics is the mode shape matrix (Φ). To understand it, see Figure 1 again. It is possible to see that the blade is separated into small squares that are finite elements. Each vertex of each element is a node and it is at this point that FEM calculates the displacement due to the mode shape. As can be seen, there are many nodes for the blade and each node can present different displacements for different mode shapes. The mode shape matrix is the matrix whose number of rows i is equal to the number of selected sensors and the number of columns j is equal to the number of mode shapes to be considered. Therefore, element a_{ij} is the displacement of node i in mode shape j.

Therefore, one of the main metrics is the KE. It gives a measure of the dynamic contribution of each element of FEM to each of the mode shapes and can be calculated through Equation (5).

$$KE_{ij} = \Phi_{ij} \sum_{j} M_{ij} \Phi_{ij} \omega_j^2 \tag{5}$$

where Φ is the mode shape matrix, M is the mass matrix, i and j refers to the degrees of freedom and n, the n-th mode (Heo *et al*. [1997]). Note that the calculated kinetic energy grows with the square of the natural frequency of the considered mode shape, so the method tends to value higher frequency nodal displacements.

Efi is one of the most used metric in large structures, which is an efficient unbiased estimator. Its objective is to select positions of measurements linearly independent providing high information. The covariance matrix of the estimated error can be expressed in Equation (6). Note that unlike KE, mass and natural frequency are not considered.

$$EfI = diag(\Phi \left[\Phi^T \Phi \right]^{-1} \Phi^T) = diag(QQ^T) \tag{6}$$

where Q is an orthonormal matrix and Φ is the mode shape matrix. This metric has a few drawbacks: *i*) it might choose sensor locations with less energy content, just like KE, what can leave sensing incomplete and bring vulnerability in noisy conditions (Cao *et al*. [2020]), *ii*) it presented poor results under conditions of uncertainty (Kammer [1992]).

The ADPR provides a measure of the contribution of any point to the global response. For all N mode shapes, the ADPR in the i-th node can be calculated using Equation (7).

$$ADPR_i = \sum_{i=1}^{N} \frac{\Phi_{ij}^2}{\omega_j} \tag{7}$$

where ω_j is the j-th natural frequency and Φ is the mode shape matrix.

The EVP calculates the product of the mode shapes for its locations for N modes to be measured: a maximum for this product is a point with optimum measurement candidate. In the i-th, it can be calculated by Equation (8):

$$EVP_i = \prod_{j=1}^{N} \left|\Phi_{ij}\right| \tag{8}$$

IE is an efficient metric to finding the best combination of structural tests that can minimize the negative consequence of uncertainty. The metric is based on a Bayesian statistical method, where a probability density function $p(\Theta|D)$ (Equation 9) is used to quantify the uncertainties in the parameters Θ. The calculation is defined in Equation (10).

$$p(\theta \mid D) = c\left[J(\theta; D)\right]^{-(NN_0-1)/2} \pi_\theta(\theta) \tag{9}$$

$$H(D) = E_\theta\left[-\ln p(\theta \mid D)\right] = -\int p(\theta \mid D) \ln p(\theta \mid D) d\theta \tag{10}$$

where E_Θ is the mathematical expectation to Θ, D is the dynamic test data, $J(\Theta|D)$ is the fit measure between the measured and the response time histories, N_0 is the number of DOF of the structure and N is the number of sampled data. Note that, while EfI gives the relative importance of the chosen DOF, IE is related to the total maximum limit of entropy.

The FIM is the main metric used in SPO, where the optimal sensor configuration is taken as the one that maximizes the norm of the FIM and minimizes the expected Bayesian loss function involving the trace of the inverse of the FIM (Gomes *et al.* [2018]). The array of sensors can be given in the form of an estimation problem with a corresponding FIM given in Equation (11) (Kammer [1991]). The modal response is estimated based on the data measured by the sensors.

$$Q = \Phi_S^T W \Phi_S \tag{11}$$

where W is a weighting matrix and Q, when maximized, results in the minimization covariance matrix error. This results in the maximization of the signal intensity and the independence of the main directions (Rao *et al.* [2015]). This metric showed good performance in noise and multi-axial data (Kammer [1992]; Kammer & Tinker [2004]).

MAC is a metric proposed by Carne and Dohrmann [1994] that aims to find sensor locations to ensure that all inner products between distinguishable shape vectors have relatively small cosines. It allows comparison of the different mode shapes and is defined by Equation (12).

$$MAC = \frac{(\Phi_i^T \Phi_J)^2}{(\Phi_i^T \Phi_i)(\Phi_j^T \Phi_J)} \tag{12}$$

where Φ_i and Φ_j are the *i*-th and *j*-th column vectors in matrix Φ. The matrix MAC values range between 0 and 1, where 1 indicates a high similarity between the modal vectors. In an ideal condition, the MAC matrix has is null and all elements of main diagonal are 1. So whether it's an OSP or damage identification problem, it is desired to maximize the sum of diagonal values. Note that EfI is MAC^{-1} (Tan & Zhang [2019]).

Many studies show significant correlation and statistical equality between: *i*) EfI, KE, and FIM, and *ii*) MAC and IE (Li *et al*. [2007]; Yi & Li [2012]). Gomes *et al*. [2018b] also found a strong correlation between the metrics FIM, KE, EI, EVP and ADPR when studying them for OSP in a laminate composite plate. The authors also conclude that EfI presented the worst result among the metrics compared. Table 1 summarizes and shows the objective functions derived from these metrics to be used in SPO or Damage Identification.

Table 1: Sensor placement objective functions used in Structural Health Monitoring

Metric	Objective function
KE	$J = max(KE)$
EfI	$J = max(diag(QQ^T))$
ADPR	$J = max(ADPR)$
EVP	$J = max(EVP)$
IE	$J = min(H(D))$
FIM	$J = max\|det(Q)\|$
MAC	$J = max(diag(MAC))$

2.4 Lichtenberg and Multi-objective Lichtenberg algorithms

With the objective function defined, meta-heuristics such as GA, PSO, DE, FA, or SFO can be applied. As shown, they are the best and most used optimization algorithms for complex problems. In the MRB SPO problem of this chapter, the Lichtenberg Algorithm (LA) (Pereira *et al*. [2021a]) will be applied, when mono-objective. The LA is a powerful meta-heuristic inspired by the physical phenomenon of intra-cloud lightning and Lichtenberg figures and is the first hybrid algorithm in the literature that combines population and trajectory optimization routines at the same time.

The meta-heuristic, also developed at GEMEC, has been successful in identifying cracks (Pereira *et al*. [2020]) and delaminations (Pereira *et al*. [2021]), isogrid tube optimization (Francisco *et al*. [2020]; Pereira *et al*. [2022a]), hydrogen production optimization (Souza *et al*. [2022]), wind forecast optimization (Tian & Wang [2022]), parameter optimization in manufacturing processes (Challan *et al*. [2022]; Mohanty *et al*. [2022]), and multi-objective optimization (Pereira *et al*. [2022]), among other applications. The LA algorithm in the mono-objective version has already been well explained in previous chapters. In this chapter, the Multi-objective Lichtenberg Algorithm (MOLA) will be presented and used in the multi-objective SPO. It is the first multi-objective meta-heuristic created and registered in Brazil.

The algorithm optimizes by creating Lichtenberg Figures (LF) that are thrown into the search space (of design variables) with random sizes and rotations at each iteration. In the mono-objective version, the LF was always centered on the best point of the previous iteration, or on the best point of all iterations so far. In the multi-objective version, these figures are triggered from some point of the variables that make up the current Pareto front. As the LF is made up of many points, only a *Pop* (population) number is randomly selected in this structure to be evaluated in the objective functions.

As the LF has different sizes in each iteration, sometimes it is small and favors exploitation, sometimes it is large and favors exploration. At each iteration, the new and old solutions are compared using the Pareto dominance relationship, thus constituting the current Pareto front. The algorithm stops when all N_{iter} iterations are complete. See Figure 2. Figure two shows the relationship between the search space (of variables) and the objective space (where the Pareto front is). Different colors show the LF in different iterations.

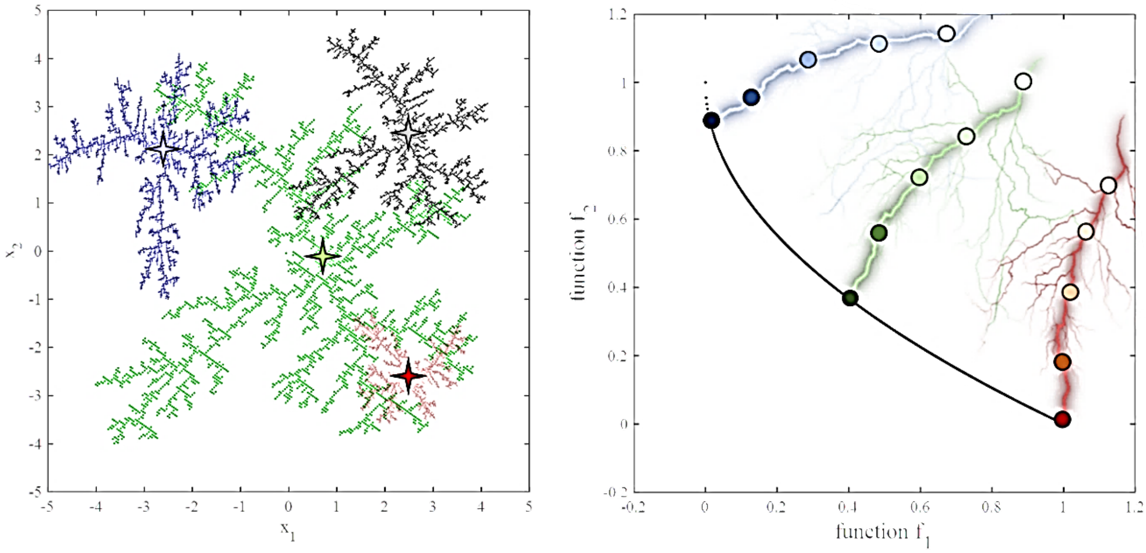

(a) Search Space (b) Objective Space

Figure 2: MOLA in a problem of two design variables and two objectives (PEREIRA *et al.*, 2022)

This is the general functioning of MOLA, however, it has other parameters besides *Pop* and N_{iter}. Three parameters control the LF creation: creation radius (R_c), number of particles (N_p), and sickness coefficient (S). The first two are associated with the size ta LF, which grows in a matrix space whose number of rows and columns is equal to twice R_c. N_p defines the number of particles or unitary elements that can be in this matrix space, remembering that it can be less than the set if the cluster of unitary values reaches R_c. S controls the density of the LF, being close to zero very dense (reminiscent of a cloud) or not, when close to 1, causing a faster cluster growining.

The LF creation process can take about 2 minutes, which would make the optimization process slow. Then another parameter called M was created that controls the creation of the LF and brings three options: *i*) The LF can be created only once and used in all iterations (M = 1), *ii*) an LF can be created at each iteration, which is not recommended (M = 2), or *iii*) an LF with optimized R_c, N_p and S values can be loaded and in this case the entire optimization process can take less than 1s (M = 0). Another additional parameter is the Ref, which creates a local LF at a ref size of the global one, always having half of all Pop, which favors exploitation. See Figure 3 of the actual LF in the search space.

Finally, it has two last parameters of MOLA related to the control of the algorithm in the construction of the Pareto front and they greatly increases its execution: the number of grids (N_{grid}) and the number of admissible solutions in the Pareto front (N_s). The first parameter divides the objective space into N_{grid} hyper cubes, decreasing the regions of comparison and analysis of the Pareto dominance relationship (Coello *et al*., 2004). N_s limits the number of solutions in the PF excluding those that are close. Therefore, MOLA has 8 parameters: Pop, N_{iter}, R_c, N_p, S, ref, N_{grid}, and N_s. Figure 4 summarizes MOLA.

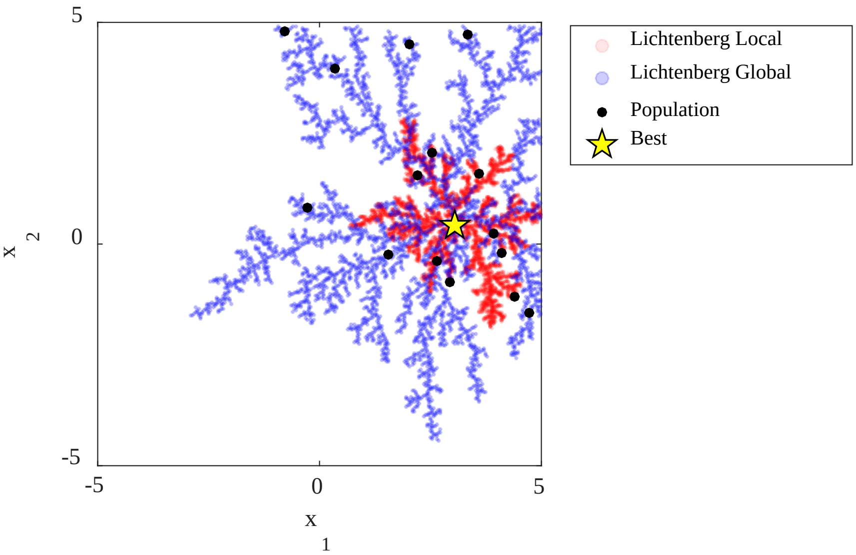

Figure 3: Lichtenberg Figures at one random iteration (*pop* = 15 and *ref* = 0.4) (PEREIRA *et al*., 2022a)

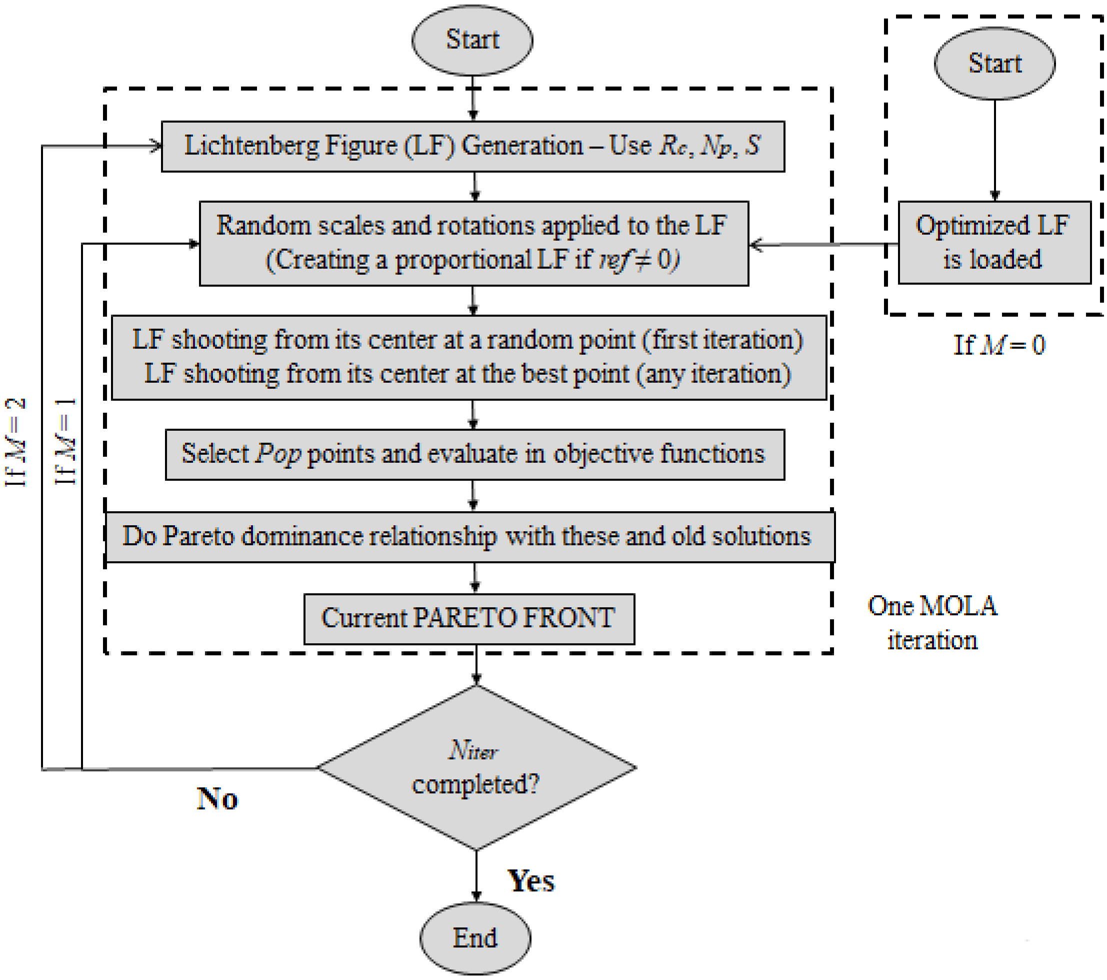

Figure 4: MOLA flowchart (PEREIRA *et al.*, 2022a)

3 Helicopter Main Rotor Blade Case Studies

The metrics discussed in Section 2.3 associated with meta-heuristics in the form of objective functions have been the most accurate and efficient approach used in SPO. As discussed in the introduction to this chapter, the vast majority of workers use a mono-objective meta-heuristic to solve one of the objective functions in Table 1 for any type of structure. However, a new technique was developed by GEMEC using feature selection for multi-objective SPO in which the number of sensors is placed as one of the objectives. In this section, studies will be carried out using both approaches, mono and multi-objective SPO, in a helicopter MRB. For this, a blade identical to an AS-350 MRB was created using FEM. See the real model in Figure 5.

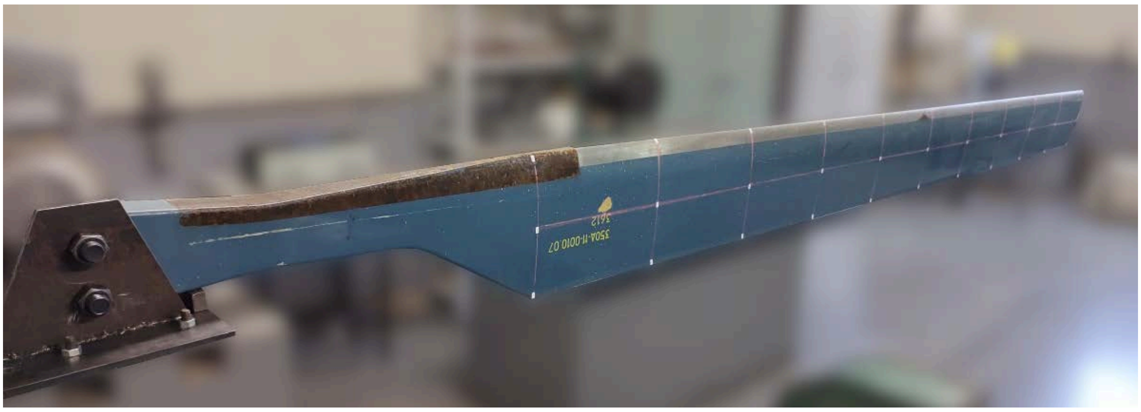

Figure 5: AS-350 MRB (Pereira *et al*. [2022b])

For this, a blade identical to an AS-350 MRB was created using FEM. The model was created in the ANSYS® APDL software and has a total length of 4665mm, being 3880mm with a NACA0012 aerodynamic profile. The element used was the SHELL281 with 8 nodes and 6 degree of freedom per node. Figure 6 shows the solid and all elements and nodes, being each node a candidate position for sensor positioning. Figure 1 showed the first 5 blade mode shapes for this numerical model.

a) Surface Model

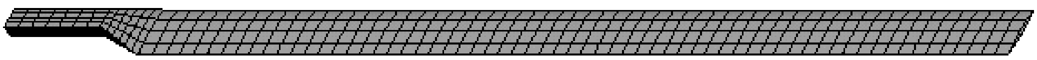

b) 746 Elements

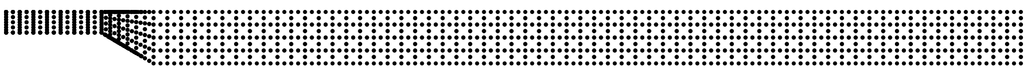

c) 2266 Nodes

Figure 6: Numerical AS-350 MRB (adapted from Pereira *et al*. [2022b])

3.1 Mono-objective sensor placement optimization

The problem of mono-objective optimization using meta-heuristics consists of some basic steps: *i*) definition of the meta-heuristic to be used and configure its parameters, mainly population and number of iterations; *ii*) definition of the objective function that will guide the optimizer in the search for optimal solutions, *iii*) definition of upper and lower bounds (LB and UB), which define the search space in which the meta-heuristic will look for the best solutions. In this way, each variable in the problem will have a search range; and *iv*) definition of the constraints of the problem, if any.

In SPO, the objective function F can be any of those in Table 1, the variables are the number of sensors n to be allocated, $\vec{\boldsymbol{X}} = \{ S_1 , S_2 , \dots , S_n \}$. The lower and upper bounds are all the numbers of nodes available in the structure, in the MRB case (Figure 2c), from 1 to 2266. Then each of the variables will have an LB of 1 and a UB of 2266, whose vector length is equal n to be positioned. In this case, it is also convenient to add a constraint g_1 that prevents sensors from overlapping, that is, so that two sensors are not positioned in the same place.

Another decision that the SPO problem operator must address is how many mode shapes he will consider. It could be just the first, it could be a multi-objective optimization considering more than one if they are conflicting, or composing an objective function that is the sum of the m mode shapes to be considered, as will be adopted here. The criterion adopted to consider the 5 modes of Figure 1 is that an MRB in the field has excitations ranging from 0 to 25 Hz (Tamer *et al.* [2021]). The SPO problem considering mono-objective optimization and KE metric is expressed in Equation 13.

$$\begin{gathered} \max F(\boldsymbol{X}) = \sum_{i=1}^{m} KE_i \\ \textit{subject to:} \\ 1 \leq \boldsymbol{S_n} \leq 2266, \textit{ for } n = 1, 2, \dots, n \\ g_1(\vec{\boldsymbol{X}}) = S_n - S_{n+1} > 1 \end{gathered} \tag{13}$$

The LA parameters used in this chapter are those in Table 2, they are optimal parameters found by the authors. Table 1 consists of 7 objective functions. Equation 10 brings the SPO problem to the first one (KE). Note that the number of sensors that will be allocated must be defined before starting the optimization process. In this chapter, 5 sensors will be considered, as it is equal to the mode shapes number being used, a minimum recommendation in the literature (Gomes *et al.* [2018]). Applying the LA with the Parameters in Table 2 for each of these metrics and considering 5 sensors, we have after seven simulations the results in Figure 3. The reader is invited to compare the mode shapes of Figure 1 with the results of Figure 7, remembering that all metrics seek to measure displacements in their own way.

Table 2: Tuned LA parameters

R_c	N_p	S	ref	Pop	N_{iter}
200	10^6	1	0.4	200	200

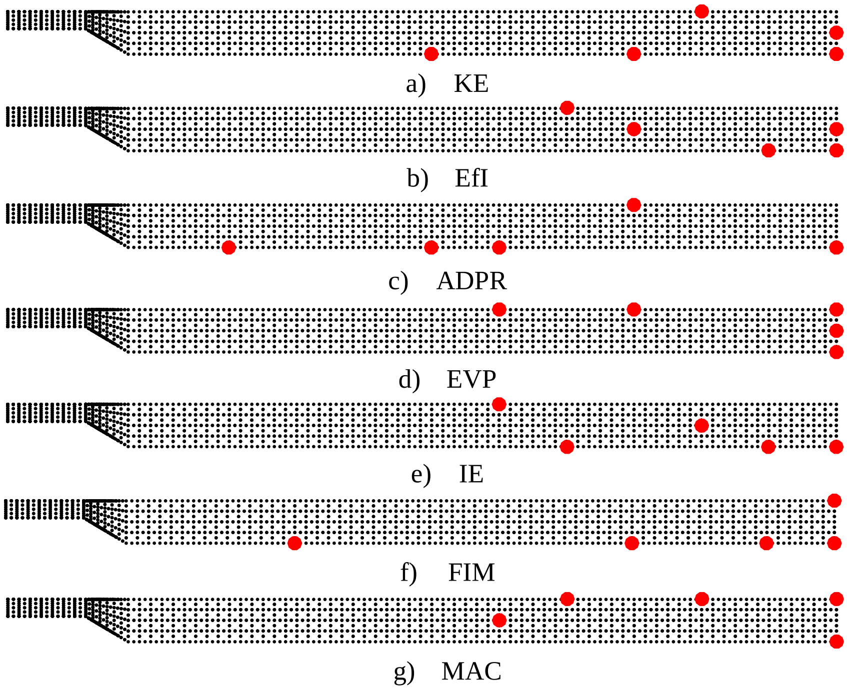

Figure 7: Sensor configurations considering 5 sensors after SPO for each metric

Since the blade is divided into three sections: root, center and tip, with the root located to the left of the images in Figure 3, it can be seen in Figure 1 that the largest nodal displacements for all mode shapes are at its tip. Then comes the central section. Considering only 5 sensors to be distributed, it can be seen that all metrics have at least one sensor at the tip, being the EVP with the highest number exactly at it. Also, all metrics selected the blade tip node that is furthest from the root support, that is, the node with the most movement flexibility of the entire MRB. All metrics have most sensors between the central region and the tip, being that only ADPR and FIM that placed a single sensor in the root section. EfI and FIM neglected the center section in relation to the other metrics. Also, as already observed in other studies in the literature, it is possible to see a sensor distribution relationship between the MAC and IE metrics and between EfI and KE, although in this case KE has considered the central section.

3.2 Multi-objective sensor placement optimization

Most of the works found in the literature perform the SPO as shown in Section 3.1. Note that for each metric or objective function, the algorithm had to be run once and the number of sensors was fixed. However, it is known that the basic principle and biggest challenge in SHM in relation to SPO is to maximize the level of information acquired from the structure by minimizing the number of sensors, which are clearly conflicting objectives.

Developing a multi-objective optimization method capable of finding a Pareto front (PF) that associates each of these metrics with the number of sensors not only allows finding a larger number of sensor configurations, since for each sensor number there will be a sensor configuration and the respective metric value, as well as allowing the problem operator to evaluate how the information level of that structure varies with the addition of sensors for that metric.

Based on this, it is possible for the problem operator for a given structure to know, for example, if the increase in the number of sensors causes the information level to grow linearly, exponentially, or parabolically. This would imply linear, convex or concave Pareto fronts. It also allows determining whether the addition of sensors allows the level of information to increase significantly up to a certain point and, from then on, it changes insignificantly. Unlike the single-objective approach, with just one execution of the SPO problem, a PF will be found that will have the best possible metric value for each integer number of sensors and each one of these solutions will have the sensors positions.

Despite being a very innovative methodology, this has not yet been done not only due to the greater programming difficulty, but also to the lack of methods. However, new techniques have been developed for data mining and filtering before machine learning algorithms training and prediction. This large area, named Feature Selection (FS), aims to minimize the number of features and maximize a model accuracy, having as its most important approach the wrapper-based method, which using meta-heuristics, it selects different subsets within the dataset and seeks to select those that present the best accuracy values (Sharma & Kaur [2021]).

In the FS problem, there is a vector of length equal to the number of original problem features, whose the selected feature worth one and the rejected, zero. Or, in this case, the sensor will be selected with a value of one and excluded with a value of zero. Therefore is a binary (and discrete) optimization problem. Here begins the first challenges, since basically all meta-heuristics are programmed to deal with continuous problems. The reader may fall into the error of thinking that a simple round could solve the problem, but this simple strategy leads to poor results.

In literature there are two main groups that can convert a optimization algorithm in binary: i) general approach, where the algorithm operators are not modified, such as transfer function and angle modulation, and ii) specific approaches, were the algorithm structure is modified, such as Boolean or quantum binary techniques (Crawford *et al.*, [2017]). The easiest and most effective is to adopt a transfer function and there are two families: *s-shaped* and *v-shaped*. See Figure 8. There are many studies comparing both and most agree that *v-shaped* transfer function is better for FS. The two main reasons for this are that this transfer function does not force continuous values to assume the values of 0 or 1 and that using it, there is a greater chance that a given feature will not be selected (Mirjalili & Lewis [2013] ; Ghosh *et al.* [2020]).

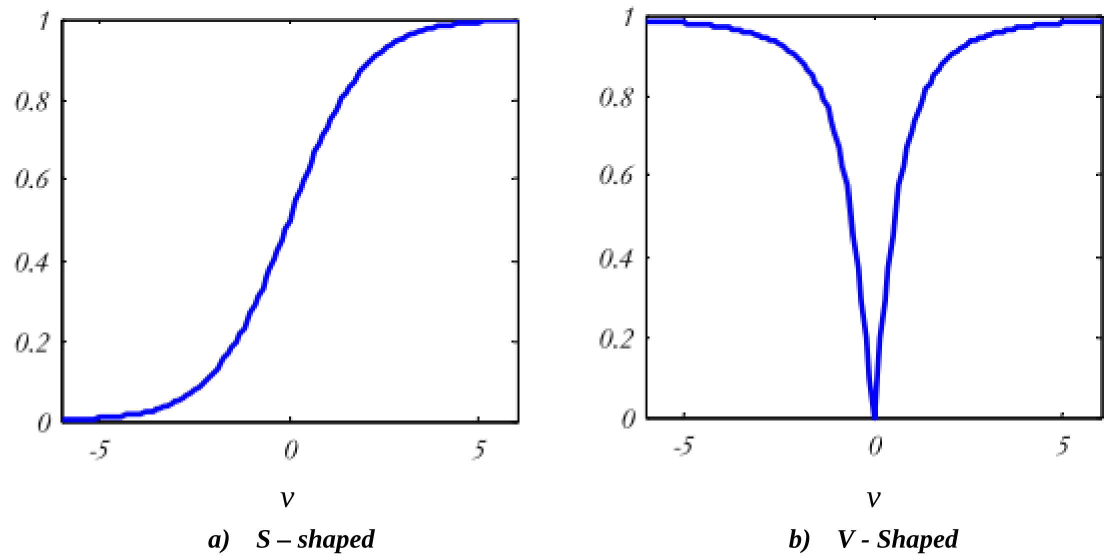

Figure 8: main groups of transfer functions

Thus, MOLA will be equipped with the *v-shaped* transfer function. The binarization process uses Equations 14 and 15 (Mirjalili & Lewis [2013]). Equation 1 represents one of the forms of this transfer function. In it, each continuous element of the vector of decision variables generated by the LA is an input.

$$T(\Delta x) = \left| \frac{\Delta x}{\sqrt{\Delta x^2 + 1}} \right| \tag{14}$$

Then, the $T(\Delta x)$ value is used in Equation 15 to calculate the probability of changing each element to 0 or 1. The *rand* is a randomly generated number between 0 and 1. When $T(\Delta x)$ has a small value, the chance of inverting the element's value is also small.

$$X_{t+1} = \begin{cases} \neg X_t, rand < T(\Delta x_{t+1}) \\ X_t, rand \geq T(\Delta x_{t+1}) \end{cases} \tag{15}$$

Implementing the *v-shaped* transfer function, MOLA becomes appropriate for the SPO problem. The node position in FEM has a integer number assigned to it, which generates a candidate sensors vector equal to the nodes number *n*, i.e., $\overrightarrow{S_c} = \{1, \ldots, n\}$. In the same way, MOLA generates a binary vector of the same length ($\vec{B}$). Through Equation 16 can be found the selected sensors vector ($\overrightarrow{S_s}$) (Pereira *et al*., [2022b]):

$$\overrightarrow{S_s} = \overrightarrow{S_c} * \overrightarrow{B^T} \tag{16}$$

For each vector $\overrightarrow{S_s}$ generated are calculated the number of sensors the metric *M* value, which can be any one of Table 1. The solutions generated in the objective space are compared through the Pareto dominance relationship and dominated solutions are excluded. That is, for a fixed number of sensors, any solution generated with worse metric values is excluded. Likewise, considering a fixed metric value, any generated solution that has a greater number of sensors for the same metric value is eliminated. The optimization problem is expressed in Equation 17 (Pereira *et al.*, [2022b]). Note that there is no way for sensors to overlap. The a_i is obtained using Equations 14 and 15 through the continuous x values between 0 and 1 delivered by MOLA.

$$F(\overrightarrow{S_s})=\left\{\min(length(\overrightarrow{S_s})\,;\max\left(M(\overrightarrow{S_s})\right)\right\}$$

where:

$$\overrightarrow{S_S} = \overrightarrow{S_C} * \overrightarrow{B^T} \qquad (17)$$
$$\overrightarrow{S_C} = \{1,\ldots,n\}$$
$$\vec{B} = \{a_1,\ldots,a_n\}$$

With the optimization problem defined in Equation 17, the binary MOLA could already be applied. However, if all 2266 nodes were considered, the problem would has an optimization problem with 2266 variables. The greater the dimensionality, regardless of the meta-heuristic to be used, more complex is the optimization problem. Looking at Figure 6c, it is possible to notice the number of extremely close nodes and obviously, not all of them need to be evaluated. Therefore, some simplifications can be made to improve the optimization process. 34 well-spaced and distributed sensors will be considered. They composed the vector of candidate sensors $\overrightarrow{S_C}$ and are represented in Figure 9.

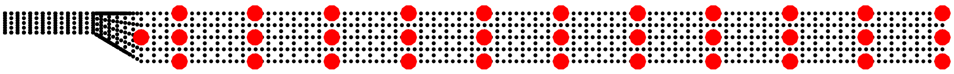

Figure 9: Candidate nodes for sensor allocation (Pereira *et al.*, [2022b])

Another important consideration and simplification of this work is that, as can be seen in Figure 1, the MRB has vibration modes with spatial displacements, that is, in all directions. Knowing that the FEM delivers the nodal displacements in the x, y and z directions, the total displacement will be considered in the optimization problem, calculated using Euclidian distance.

Having defined the optimization problem of Equation 17 and adopted some simplifications strategies, the binary MOLA can be applied with the parameters of Table 3 for all the objective functions of Table 1, considering the first five mode shapes of the MRB, resulting in 7 multi-objective optimization problems. In Pereira *et al.* [2022b] was considered the first six mode shapes and this methodology was called Multi-objective Sensor Selection and Placement Optimization based on Lichtenberg Algorithm (MOSSPOLA). Just for the reader to have an idea, for each of these problems, MOSSPOLA tested 200 x 200 = 40000 sensor configurations in an average time of 18s. And just in this single run it will try to find at least one sensor configuration for each number of sensors, unlike the traditional SPO methodology that the number of sensors is fixed and therefore each program run is limited to only this number of sensors. The Pareto fronts found are shown in Figure 10.

Table 3: Tuned MOLA parameters

R_c	N_p	S	ref	Pop	N_{iter}	N_{grid}	N_s
200	10^6	1	0.4	200	200	30	100

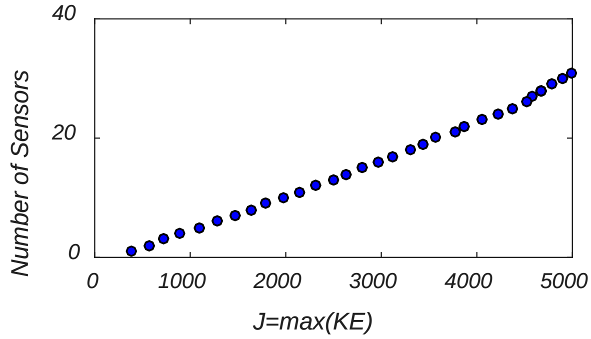

a) Kinetic Energy

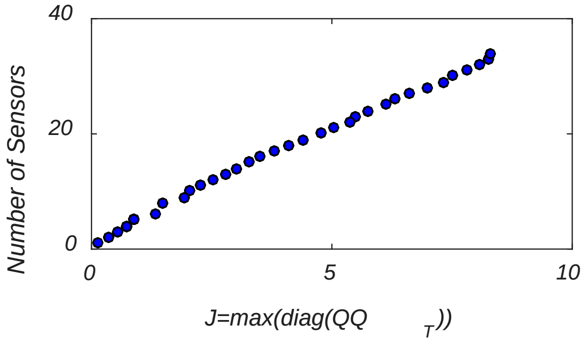

b) Effective Independence

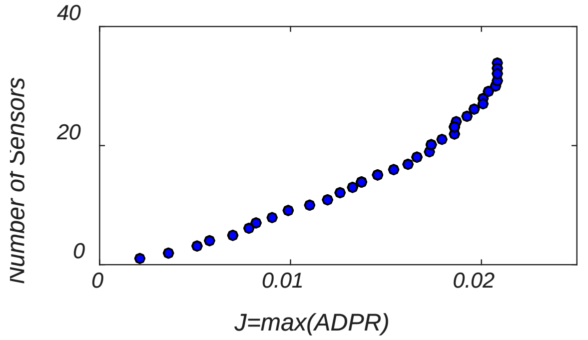

c) Average Driving-Point Residue

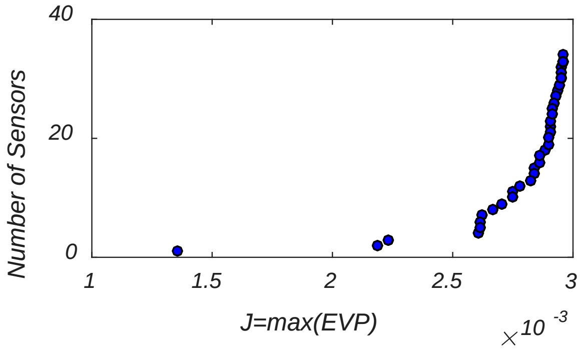

d) Eigenvalue Vector Product

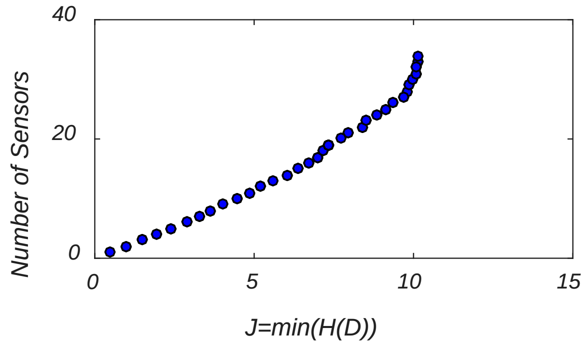

e) Information Entropy

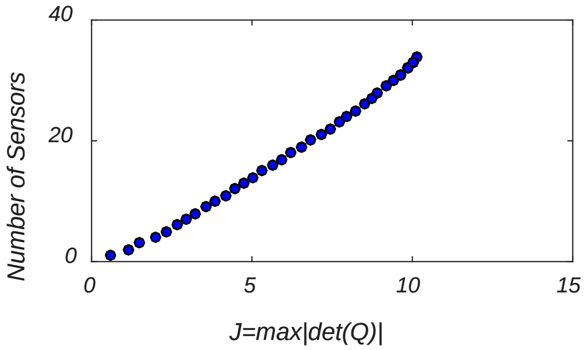

f) Fisher Information Matrix

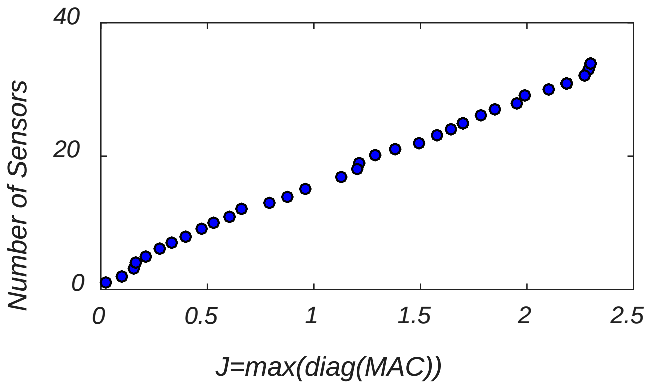

g) Modal Assurance Criterion

Figure 10: Answering how MRB information varies with the number of sensors using Pareto front for seven SPO metrics and the first five mode shapes

Interesting discussions can be made from Figure 10, remembering that these Pareto fronts refer exclusively to the MRB and its first 5 mode shapes. The first is that the applied methodology was able to successfully find at least one sensor configuration for each number of sensors in all metrics. It was also noticed that for all metrics, the increase in the number of sensors will always lead to an increase in the level of information acquired from the MRB.

For the KE, EfI, and FIM metrics, the MRB information level grows linearly with the increase in the number of sensors up to the number 34, the interval used in this study. Already the ADPR, IE, and MAC metrics have a smoothly convex behavior and in both the information level does not significantly improves from 25 sensors. The EVP metric was the one that showed the most information gain for the first 4 sensors, and from this the information level does not grow significantly anymore too. Still, it is possible to confirm with this methodology the relationship between some metrics, already found in other studies: *i*) EfI, KE, and FIM (Gomes *et al*. [2018b]; Li *et al*. [2007]), and *ii*) MAC and IE (Yi & Li [2012]).

Each solution of these Pareto fronts has a sensor configuration with its number and positions. It would be exhausting and tiring to present every sensor configuration found for every metric. Considering that the number of mode shapes used is 5 and it is recommended that the number of sensors used is at least equal to this number, Figure 11 shows all solutions for 5 sensors. Figures 12 and 13 bring the solutions for 7 and 9 sensors respectively. Remembering that good damage identification (delamination) results have already been found using only 10 well-distributed sensors without any SPO study (Gomes *et al* [2020b]). The scale that shows the distances of the sensors on the blade is in meters.

It is possible to see that in Figures 11, 12 and 13 that again all metrics allocate at least one sensor at the end of the MRB, with the IE for five sensors (Figure 11e) being the only one that not selected the node at the lower tip, furthest from the root base and point of greater flexibility. Can be also seen that the metrics still prefer to select nodes in the central and tip regions, with the ADPR metric being the only one to select at least one point in the root section in all cases. And this pattern remains even increasing the number of sensors (from 5 to 7 and 9).

Figure 11 represents the multi-objective SPO solutions for 5 sensors, which can be compared with the 5-sensor solutions of the single-objective SPO of Figure 7. Can be seen that the sensor configurations for the metrics KE, EfI, ADPR, EVP, and IE are very similar, though not identical. As for the FIM metric, although both allocated more than 40% of the sensors in the tip, in the multi-objective version it is clear that the metric allocated more sensors in the central region. The opposite happened with the MAC, which in the multi-objective version allocated even more sensors in the tip than in the central section. These are not significant differences, but they did happen.

Therefore, still discussing Figure 11, KE, ADPR, EVP, and FIM were the only metrics that had better sensor distribution, as they divided the available sensors well in the most energetic regions of the blade, at the extreme tip and exactly in the middle. Therefore, still discussing Figure 11, KE, EVP and FIM were the only metrics to distribute the sensors well in the regions of greater displacement, center and tip. Again, the APR metric was the only one to allocate sensors at the root and the MAC metric was the one that put the most sensors at the tip.

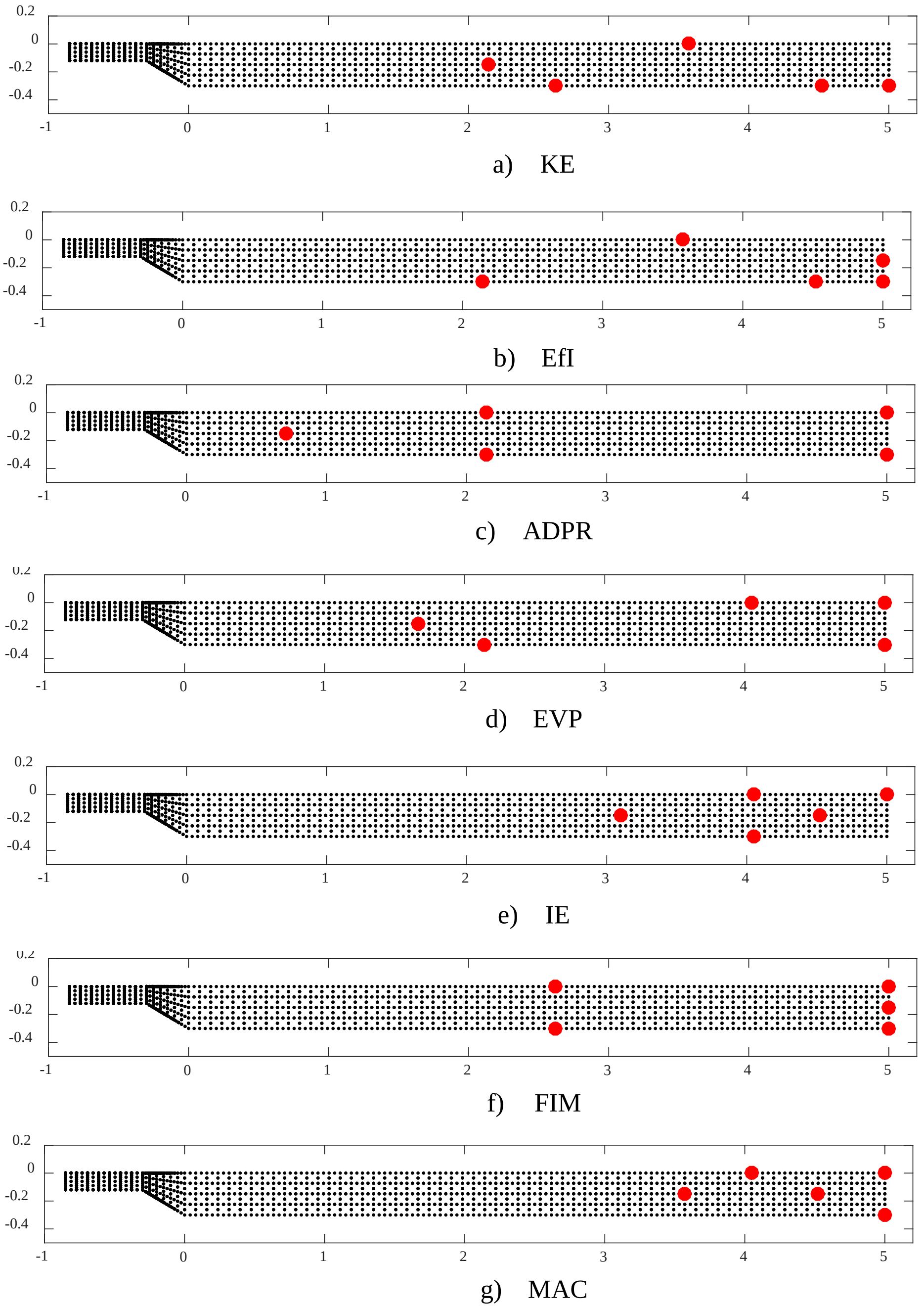

Figure 11: Best sensor configuration for five sensors in different SPO metrics.

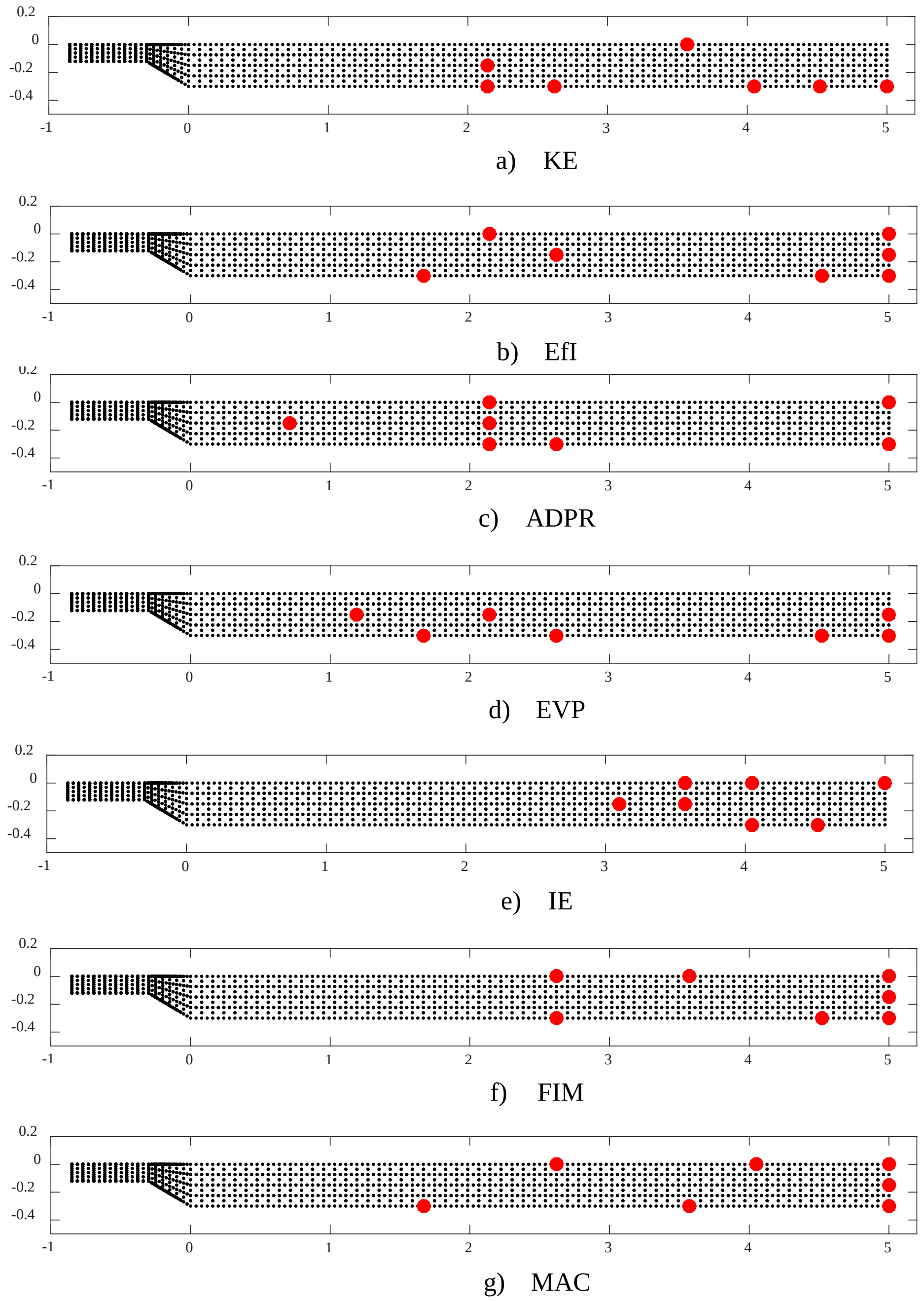

Figure 12: Best sensor configuration for seven sensors in different SPO metrics.

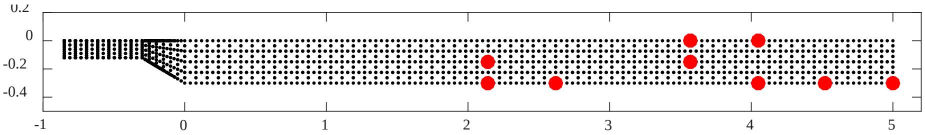

a) KE

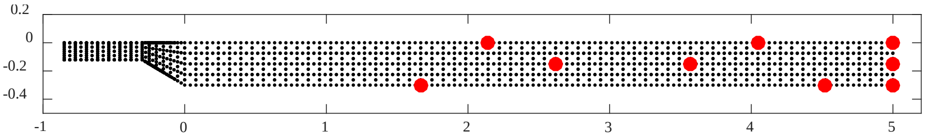

b) EfI

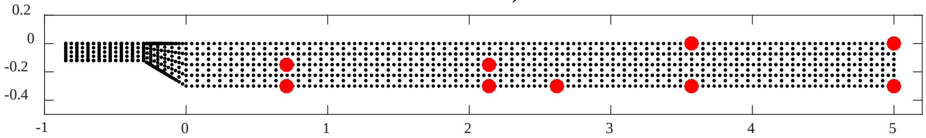

c) ADPR

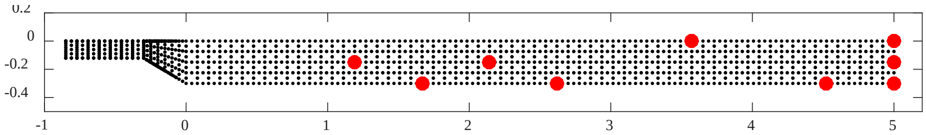

d) EVP

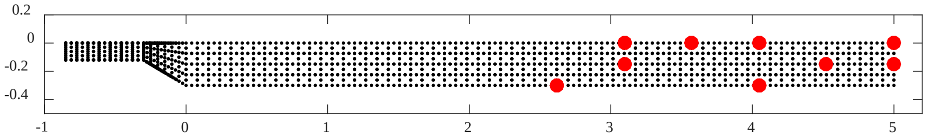

e) IE

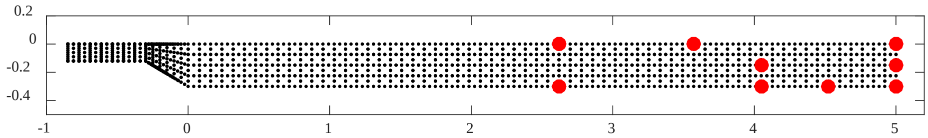

f) FIM

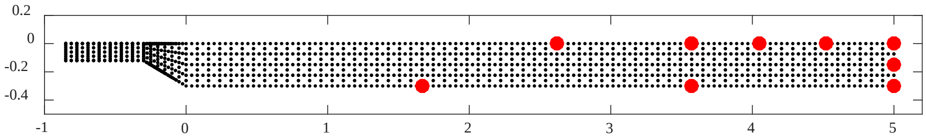

g) MAC

Figure 13: Best sensor configuration for nine sensors in different SPO metrics.

Increasing the number of sensors to 7 (Figure 12), all metrics maintain the same sensor distribution pattern, with the exception of MAC and EfI, which better distributes sensors between the central and root sections. Note that as shown in the Pareto fronts of Figure 10, these metrics have increased sensing in the central region, raising the information level of the entire blade. So, these join the metrics KE, EVP and FIM, which continue to have the best sensor distributions. IE continues to place all sensors in the tip section and ADPR still has two sensors at the tip and the majority between the root and beginning of the central section. The EVP metric now has sensors closer to the root. Considering 9 sensors, the offer of sensors is considerable and all metrics are distributed more evenly between the higher displacement sections of the blade. However, the IE and FIM metrics continue to allocate most of the sensors between the exact middle of the blade and the tip, smoothly accompanied by the MAC.

Being damage identification the main purpose of sensing, it is known that in general, the closer the damage is to the sensor, the easier it is to diagnose. Therefore, a good distribution of sensors implies in a more efficient HUMS for all blade sections. The only metrics that had a good sensors distribution for the number of sensors analyzed and at the same time always had a greater allocation of sensors in regions with greater displacements due to mode shapes were KE and EVP.

Figure 14 shows how the sensor distribution is modified for different numbers of sensors for these two metrics, starting from 1 to 30 sensors. As discussed before, the node with the greatest flexibility and therefore the greatest range of motion is at the tip, at the vertex opposite to the blade attachment by the root, and both metrics consider this point as the point of maximum information for a single sensor. From then on, the EVP metric allocates more sensors exactly at the tip and at the same time it is the one that has sensors closer to the root. Therefore, because it is more distributed, the EVP metric has the lowest sensor density. However, both highly value the tip and center sections.

The EVP and KE metrics seem to be the most suitable for the MRB. The sensor configurations for 5 sensors considering mono and multi-objective optimization and for 7 and 9 sensors considering multi-objective optimization were presented for these metrics and for others 5 important metrics in literature.

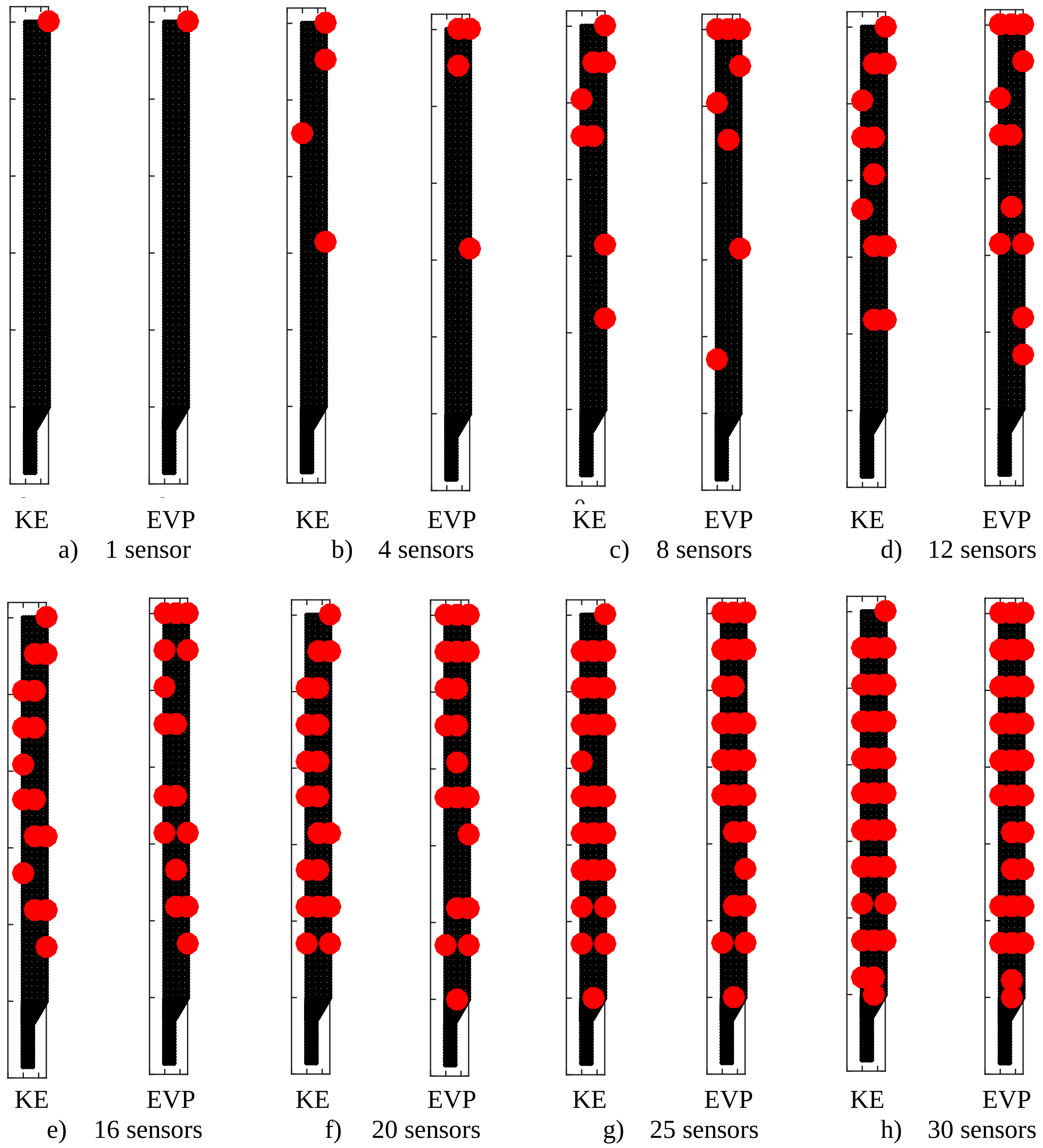

Figure 14: Sensor distribution variation as increases the sensors number

4 Concluding Remarks

This chapter showed the relevance of using rotary-wing aircraft and focused on the study of damage to its main component: the main rotor blade. A discussion of the types of damage that ranged from blade manufacture to damage that can arise in use was made. It also detailed how modal data can help engineers analyze the presence of damage in structures and showed how the study of sensor positioning is crucial for a good Health and Usage Monitoring System. This chapter presented the main sensor placement optimization metrics most used in the literature, this chapter used mono and multi-objective optimizations to find the best sensor configurations for the blade. The techniques used were developed in the Research Group in Computational Mechanics (GEMEC) at UNIFEI.

5 Perspectives for Future Research Work

The future research suggestions in this chapter relate mainly to two fronts: continuation of the SPO theme and adjustment of the numerical model in the FEM to better fit the reality of the MRB.

5.1 Sensor placement optimization continuation

The study of SPO in MRB carried out in this chapter follows the line of more recent works for different structures in the literature. A meta-heuristic is employed and the objective is to find the sensor positions that have the largest displacements for the mode shapes to be considered. Obviously, these positions will also represent the most significant changes in a possible damage presence. Furthermore, in the optimization process, only the mode shapes and natural frequencies of a single FEM simulation are considered: the healthy and intact blade. This brings one of the main advantages of this methodology: finding sensor configurations in complete optimization simulations in less than 3 minutes.

However, this methodology is unable to answer, for example, which of all sensor configurations in Figures 7, 11, 12, and 13 is more accurate in finding damage in any blade section. Could the accuracy of a specific sensor configuration change for damage in different regions? Could sensor configurations that are more present in the tip section be better at diagnosing damage anywhere on the blade? The answers to these questions can only be confirmed after damage identification studies using the sensor configurations found.

In this case, meta-heuristics have also been widely applied, but the objective functions may be different from those in Table 1, although they can also be used. In this case, Equation 4 can be used in the FEM to induce damage with well-defined intensity (α) and location (n_e) in any structures with N_e elements, with the damage rate varying between 0 and 100% (structure intact). An example of objective function widely used to guide the meta-heuristic in a damage identification problem is represented in Equation 18, where this optimization problem is also defined (Pereira *et al.* [2021]).

$$\min\ J_\Phi = \sum_{i=1}^{n} \sqrt{\left(1 - \frac{\Phi_{i,s}^{MH}}{\Phi_{i,s}^{real}}\right)^2}$$

subject to: (18)

$$1 \le \boldsymbol{n_e} \le N_e$$

$$0 \le \boldsymbol{\alpha} \le 1$$

where $\Phi_{i,s}^{MH}$ are the nodal displacements in mode shape *i* in the sensors found in the SPO problem for random damages suggested by some meta-heuristic and $\Phi_{i,s}^{real}$ is the reading of the nodal displacements in the real structure in the same node positions, which could be the MRB. Or, if it's a numerical simulation problem, $\Phi_{i,s}^{real}$ could be the displacement data of the mode shapes using the same FEM structure with a known and induced damage. The meta-heuristic optimizes suggesting damages, calculating their modal data, and comparing them with the real one. When the difference is zero, the damage will be identical. Note that for each point in the population in each iteration, the FEM is activated, which makes the optimization process to identify damages computationally expensive. A single simulation can take just over a day.

Nonetheless, this is the only way to validate the accuracy of the sensor configurations found. In normal way and as has been discussed in the literature, each of the sensor configurations of Figures 7, 11, 12, and 13 can have three damages induced in the root, tip and center sections. At least S simulations can be run for each damage and each sensor configuration and can be calculated which of these had the smallest error in relation to α and n_e. A similar way frequently used referring mainly to n_e is the Probability of Detection (PoD) (Diacenco [2016]). This is a measure that is the rate of times that the optimization problem of Equation 18 was executed and found the exact location of the damage n_e in relation to all trials, which can also be used as an objective function to be maximized.

Therefore, two interesting directions can be suggested in relation to the SPO study in this chapter, in order of increasing computational cost: *i*) Do a general damage identification study with the sensor configurations found in Figures 7, 11, 12, and 13 to see which has the smallest error or the largest PoD and *ii*) Use the methodology presented with MOLA and Feature Selection for multi-objective SPO and for each sensor configuration proposed, run the optimization problem of Equation 18 S times and calculate the PoD or error, which will be the second objective function instead of the main SPO metrics. Note that it may have an exhausting computational cost, but to the best knowledge of the authors it has never been done before and it can bring promising results, since the first objective is the number of sensors.

Some suggestions regarding the algorithms can also be presented: *i*) Test other meta-heuristics in place of MOLA and compare the results of Figure 10 using robust metrics for comparison of Pareto fronts when there is no true Pareto front as a reference, such as HyperVolume (Kumar *et al*., [2021]), *ii*) Use chaos theory or lévy flights in MOLA to try to improve the Pareto fronts results, *iii*) Test other methods of binarizing the continuous values of MOLA and also compare Pareto fronts to try to improve the results, *iv*) apply binary MOLA on different/new SPO metrics, *v*) apply the SPO methodology presented in different structures, since both the method and the application in MRB are new and have not yet been applied in any other structure. This includes repeating all previous items, among others.

5.2 Improvement of the finite element method and its alignment with reality

Still on the continuations of the SPO problem presented in this chapter, future suggestions can be added regarding modeling in FEM. Although a numerical model of the MRB with NACA0012 profile and geometric characteristics similar to the real AS-350 blade was used, to the detriment of many works in the literature that used simply a beam, simplifications were made and may influence the SPO result.

As can be seen in Figure 6a, the MRB is simply fixed by the root surface and fixation by screws in the head rotor, which usually have a metallic jacket, was not modeled. Still, in fact, the MRB is connected to the hub via three rings (and Degrees of Freedon):

flapping, drag, and pitch-change, which allows movement in these same directions in flight. See Figure 4.

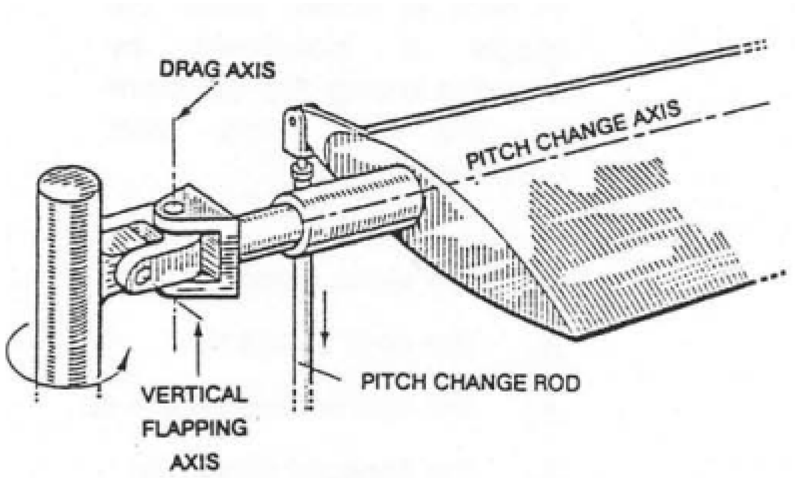

Figure 15: Axes of freedom for the MRB (Bramwell et al. [2001])

Still comparing Figures 6a and 5, it is also possible to observe that some sections have a spline for corner smoothing, which is also not included in the numerical model. The same occurred with the leading edge that has a protective steel frame. These are geometric and boundary conditions details.

The following simplification can significantly affect the SPO results and is about the dynamic modeling. As seen and discussed, the natural frequencies and mode shapes were calculated considering that the blade is simply static and supported by the root at the hub. However, there are several sources of forces and vibrations in a helicopter in flight and can change the MRB rigidity. The most important is the centrifugal force due to the rotation of the rotor. With it, a traction stress is added to each element of the blade, getting bigger from the tip to the root section of the MRB.

The common and unavoidable sources of vibrations in the main blade that would be welcome at the FEM are: *i*) variable aerodynamic forces resulting from the cyclic movement of the blades in translational flight, *ii*) centrifugal forces from the center of gravity variation position due the flapping motion of the blades, and *iii*) aerodynamic forces from the air flow in rotors, among others. These concepts have been better discussed in earlier chapters.

Other studies can also be done in relation to the type of induced damage. As a suggestion of section 5.1, a case study of damage identification degrading the elastic property of a single element was shown, that is widely used in literature to simulate delamination. However, other types of damage can be modeled, such as circular holes (which can represent ballistic damage) and cracks, to verify if the sensor configurations found are capable of diagnosing them.

Acknowledgements

The authors would like to acknowledge the financial support from the Brazilian agency CNPq (Conselho Nacional de Desenvolvimento Científico e Tecnológico), CAPES (Coordenação de Aperfeiçoamento de Pessoal de Nível Superior), and FAPEMIG (Fundação de Amparo à Pesquisa do Estado de Minas Gerais - APQ-00385-18).

References

Ahmad, K., Baig, Y., Rahman, H., & Hasham, H. J. (2020). Progressive failure analysis of helicopter rotor blade under aeroelastic loading. Aviation, 24(1), 33-41.

Alkayem, N. F., Cao, M., Zhang, Y., Bayat, M., & Su, Z. (2017). Structural damage detection using finite element model updating with evolutionary algorithms: a survey. Neural Computing and Applications, 30(2), 389–411.

Amafabia, D. Montalvão, O. David-West, G. Haritos, A Review of Structural Health Monitoring Techniques as Applied to Composite Structures, in SDHM Structural Durability and Health Monitoring, Vol. 11, No. 2, pp. 91-147, (2017).

Assis, F. M., & Gomes, G. F. (2021). Crack identification in laminated composites based on modal responses using metaheuristics, artificial neural networks and response surface method: a comparative study. Archive of Applied Mechanics.

Barthorpe RJ, Worden K (2009) Sensor placement optimization. Encyclopedia of Structural Health Monitoring.

Benner P, Herzog R, Lang N, Riedel I, Saak J (2017) Comparison of model order reduction methods for optimal sensor placement for thermo-elastic models.

Bramwell, A.R.S., Done, J., Balmford, D., “Bramwell’s helicopter dynamics”, Reed Educational and Professional Publ. Ltd, 2001, 373 p

Braun, C. E., L.D. Chiwiacowsky, A.T. Gomez, Variations of Ant Colony Optimization for the solution of the structural damage identification problem, Procedia Comput. Sci. 51 (2015) 875–884

Burgos, D. A. T., Vargas, R. C. G., Pedraza, C., Agis, D., &Pozo, F. (2020). Damage Identification in Structural Health Monitoring: A Brief Review from its Implementation to the Use of Data-Driven Applications. Sensors, 20(3), 733.

Cao, X., Chen, J., Xu, Q., & Li, J. (2020). A distance coefficient-multi objective information fusion algorithm for optimal sensor placement in structural health monitoring. Advances in Structural Engineering, 136943322096437.

Carne TG and Dohrmann CR. A modal test design strategy for model correlation. Albuquerque, NM: Sandia National Labs, 1994.

Cattarius, J., & Inman, D. J. (2000). Experimental verification of intelligent fault detection in rotor blades. International Journal of Systems Science, 31(11), 1375–1379.

Challan, M., Jeet, S., Bagal, D. K., Mishra, L., Pattanaik, A. K., & Barua, A. (2022). Fabrication and mechanical characterization of red mud based Al2025-T6 MMC using Lichtenberg optimization algorithm and Whale optimization algorithm. Materials Today: Proceedings, 50, 1346-1353.

Chen, L. Yu, A new structural damage detection strategy of hybrid PSO with Monte Carlo simulations and experimental verifications, Measurement 122 (2018) 658–669.

Coello, C. A. C., Lamont, G. B. & Lechuga, M. S. (2004). Handling multiple objectives with particle swarm optimization. Evolutionary Computation, IEEE Transactions on, 8(3), 256-279.

Colombo, M.D. Todd, C. Sbarufatti, M. Giglio. (2022). On statistical Multi-Objective optimization of sensor networks and optimal detector derivation for structural health monitoring. Mechanical Systems and Signal Processing. Volume 167, Part A , 108528. ISSN 0888-3270.

Crawford, R. Soto, G. Astorga, J. García, C. Castro, F. Paredes, Putting continuous metaheuristics to work in binary search spaces, Complexity 2 (2017) 1–19.

Diacenco, A. A. Optimization Modeling Applied to the Sensor Topology for Identification and Localization of Damages in Composite Plate (In Portuguese: Modelagem de Otimização Aplicada à Topologia de Sensores para Identificação e Localização de Danos em Placa Compósita). 2016. Doctoral Thesis, Federal University of Itajubá, MG. https://repositorio.unifei.edu.br/jspui/handle/123456789/582

Ferentinos, K. P. & Tsiligiridis, T. A. (2007). Adaptive design optimization of wireless sensor networks using genetic algorithms. Computer Networks, 51(4), 1031–1051.

Francisco MB, Junqueira DM, Oliver GA, Pereira JLJ, da Cunha SS, Gomes GF. Design optimizations of carbon fibre reinforced polymer isogrid lower limb prosthesis using particle swarm optimization and Lichtenberg algorithm. Eng Optim 2020.

Ghosh, K. K., Ritam Guha, R., Bera S. K. S-Shaped versus V-Shaped Transfer Functions for Binary Manta Ray Foraging Optimization in Feature Selection Problem. Research Square, 2020. DOI 10.21203/rs.3.rs-28684/v1

Ghoshal, A., Harrison, J., Sundaresan, M. J., Hughes, D., & Schulz, M. J. (2001). Damage detection testing on a helicopter flexbeam. Journal of Intelligent Material Systems and Structures, 12(5), 315–330

Gomes, G. F., Almeida, F. A., Silva Lopes Alexandrino, P., Cunha, S. S., Sousa, B. S., & Ancelotti, A. C. (2018). A multi-objective sensor placement optimization for SHM systems considering Fisher information matrix and mode shape interpolation. Engineering with Computers.

Gomes, G. F., S.S. da Cunha, P.D.S.L. (2018b). Alexandrino, B.S. de Sousa, A.C. Ancelotti, Sensor placement optimization applied to laminated composite plates under vibration, Struct. Multidiscipl. Optimiz. 58 (5) 2099–2118.

Gomes G. F., Sebastiao Simões da Cunha Jr., Antonio Carlos Ancelotti Jr., A sunflower optimization (SFO) algorithm applied to damage identification on laminated composite plates, Eng. Comput. 35 (2) (2019) 619–626

Gomes, G. F., & Giovani, R. S. (2020). An efficient two-step damage identification method using sunflower optimization algorithm and mode shape curvature (MSDBI–SFO). Engineering with Computers.

Gomes, G. F., Souza Chaves, J. A., & de Almeida, F. A. (2020b). An inverse damage location problem applied to AS-350 rotor blades using bat optimization algorithm and multiaxial vibration data. Mechanical Systems and Signal Processing, 145, 106932.

Gopalakrishnan *et al*. (2011) Srinivasan Gopalakrishnan, Massimo Ruzzene, e Sathyanarayana Hanagud. Computational techniques for damage detection, classification and quantification. Em Computational Techniques for Structural Health Monitoring, pages 407–461. Springer.

Guan et al. (2017) Xuefei Guan, Yongxiang Wang, e Jingjing He. A probabilistic damage identification method for shear structure components based on cross-entropy optimizations. Entropy, 19(1):27.

Hearn & Testa (1991) George Hearn e Rene B Testa. Modal analysis for damage detection in structures. Journal of Structural Engineering, 117(10):3042–3063.

Heo G, Wang M and Satpathi D. Optimal transducer placement for health monitoring of long span bridge. Soil Dyn Earthq Eng 1997; 16(7–8): 495–502

Hou, W., & Zhang, W. Advanced Composite Materials defects/damages and health monitoring, in Proceedings of the IEEE 2012 Prognostics and System Health Management Conference (PHM-2012 Beijing), Beijing, pp. 1-5, (2012).

Jin H, Xia J and Wang YQ. Optimal sensor placement for space modal identification of crane structures based on an improved harmony search algorithm. J Zhejiang Univ: Sc A 2015; 16(6): 464–477.

Kammer DC. Sensor placement for on-orbit modal identification and correlation of large space structures. J Guid Control Dynam 1991; 14(2): 251–259.

Kammer DC. Effects of noise on sensor placement for on-orbit modal identification of large space structures. J Dyn Syst 1992; 114(3): 436–443.

Kammer DC and Tinker ML. Optimal placement of triaxial accelerometers for modal vibration tests. Mech Syst Signal Pr 2004; 18(1): 29–41.

Khabarov, S. S., & Komshin, A. S. (2021). Fiber-Optic Measurement Technology and the Phase-Chronometric Method for Controlling and Monitoring the Technical Condition of Aircraft Structures. Measurement Techniques, 64(2), 131–138.

Kiddy, J., & Pines, D. (2001). Experimental validation of a damage detection technique for helicopter main rotor blades. Proceedings of the Institution of Mechanical Engineers, Part I: Journal of Systems and Control Engineering, 215(3), 209–220.

Latifi, F.P. van der Meer, L.J. Sluys, A level set model for simulating fatigue-driven delamination in composites, International Journal of Fatigue, Vol. 80, pp. 434–442, (2015)

Li D, Li H and Fritzen C. The connection between effective independence and modal kinetic energy methods for sensor placement. J Sound Vib 2007; 305(4–5): 945–955.

Lin, J.-F., Xu, Y.-L., & Law, S.-S. (2018). Structural damage detection-oriented multi-type sensor placement with multi-objective optimization. Journal of Sound and Vibration, 422, 568–589.

Milad Jahangiri, M.A. Najafgholipour, S.M. Dehghan, M.A. Hadianfard. (2019) The efficiency of a novel identification method for structural damage assessment using the first vibration mode data, J. Sound Vibr. 458. 1–16.

Mirjalili S, Lewis A (2013) S-shaped versus V-shaped transfer functions for binary particle swarm optimization. Swarm Evolut Comput 9:1–14

Mishra, S.K. Barman, D. Maity, D.K. Maiti, Ant lion optimisation algorithm for structural damage detection using vibration data, J. Civil Struct. Health Monitor. 9 (1) (2019) 117–136.

Mohanty, A., Nag, K. S., Bagal, D. K., Barua, A., Jeet, S., Mahapatra, S. S., & Cherkia, H. (2022). Parametric optimization of parameters affecting dimension precision of FDM printed part using hybrid Taguchi-MARCOS-nature inspired heuristic optimization technique. Materials Today: Proceedings, 50, 893-903.

Pan, L. Yu, Z.P. Chen, W.F. Luo, H.L. Liu, A hybrid self-adaptive Firefly-Nelder-Mead algorithm for structural damage detection, Smart Struct. Syst. 17 (6) (2016) 957–980.

Pantano, Cohesive Model for the Simulation of Crack Initiation and Propagation in Mixed-Mode I/II in Composite Materials, Applied Composite Materials, Vol. 26, No. 4, pp. 1207-1225, (2019).

Pawar, P. M., & Ganguli, R. (2003). Genetic fuzzy system for damage detection in beams and helicopter rotor blades. Computer Methods in Applied Mechanics and Engineering, 192(16-18), 2031–2057.

Pawar, P., & Ganguli, R. (2005). On the effect of matrix cracks in composite helicopter rotor blade. Composites Science and Technology, 65(3-4), 581–594.

Pawar, P., & Ganguli, R. (2007). Fuzzy-Logic-Based Health Monitoring and Residual-Life Prediction for Composite Helicopter Rotor. Journal of Aircraft, 44(3), 981–995.

Pawar, P. M., & Sung Nam Jung. (2007b). Support Vector Machine based Online Composite Helicopter Rotor Blade Damage Detection System. Journal of Intelligent Material Systems and Structures, 19(10), 1217–1228.

Pawar, P. M., & Ganguli, R. (2007c). On the effect of progressive damage on composite helicopter rotor system behavior. Composite Structures, 78(3), 410–423.

Pereira JLJ, Chuman M, Cunha SS, Gomes GF. Lichtenberg optimization algorithm applied to crack tip identification in thin plate-like structures. Eng Comput (Swansea, Wales) 2020;38:151–66. https://doi.org/10.1108/EC-12-2019-0564.

Pereira JLJ, Francisco MB, Cunha SS da, Gomes GF. (2021). A powerful Lichtenberg Optimization Algorithm: A damage identification case study. Eng Appl Artif Intell; 97:104055.

Pereira JLJ, Francisco MB, Diniz CA, Antônio Oliver G, Cunha SS, Gomes GF. Lichtenberg algorithm: A novel hybrid physics-based meta-heuristic for global optimization. Expert Syst Appl 2021a;170.

Pereira, J.L.J., Oliver, G.A., Francisco, M.B. *et al.* (2021b). A Review of Multi-objective Optimization: Methods and Algorithms in Mechanical Engineering Problems. Arch Computat Methods Eng.

Pereira JLJ, Guilherme Antônio Oliver, Matheus Brendon Francisco, Sebastião Simões Cunha Jr, Guilherme Ferreira Gomes. (2022). Multi-objective lichtenberg algorithm: A hybrid physics-based meta-heuristic for solving engineering problems. Expert Systems with Applications. Volume 187, 115939, ISSN 0957-4174.

Pereira, J.L.J., Francisco, M.B., Ribeiro, R.F. et al. Deep multiobjective design optimization of CFRP isogrid tubes using lichtenberg algorithm. Soft Comput (2022a)

Pereira, J.L.J., Francisco, M.B., Souza Chaves, J. A., Sebastião Simões Cunha Jr & Gomes, G. F. (2022b). Multi-objective sensor placement optimization of helicopter rotor blade based on feature selection. Mechanical Systems and Signal Processing. Volume 180. 109466. ISSN 0888-3270. https://doi.org/10.1016/j.ymssp.2022.109466.

Shahani, A. R., & Mohammadi, S. (2015). Damage tolerance and classic fatigue life prediction of a helicopter main rotor blade. Meccanica, 51(8), 1869–1886.

Tian, Z. & Wang, J. Variable frequency wind speed trend prediction system based on combined neural network and improved multi-objective optimization algorithm. Energy. Volume 254. Part A. 2022.

Kaveh, M. Maniat, Damage detection based on MCSS and PSO using modal data, Smart Struct. Syst. 15 (5) (2015) 1253–1270

Rao ARM, Lakshmi K, Kumar SK (2015) Detection of delamination in laminated composites with limited measurements combining pca and dynamic qpso. Adv Eng Softw 86:85–106.

Reddy, R. R. K., & Ganguli, R. (2003). Structural damage detection in a helicopter rotor blade using radial basis function neural networks. Smart Materials and Structures, 12(2), 232–241.

Santos, F. B., Peeters, H. Van der Auweraer, and L. C. S. Góes, "Experimental damage detection of a helicopter main rotor blade based on modal properties," in Proceedings of the International Conference on Structural Engineering Dynamics (ICEDyn 2013), Sesimbra, Portugal, 17–19 June 2013.

Santos, F. L. M., Peeters, B., Van der Auweraer, H., Góes, L. C. S., & Desmet, W. (2016). Vibration-based damage detection for a composite helicopter main rotor blade. Case Studies in Mechanical Systems and Signal Processing, 3, 22–27.

Sharma, Manik; KAUR, Prableen. A Comprehensive Analysis of Nature-Inspired Meta-Heuristic Techniques for Feature Selection Problem. Archives of Computational Methods in Engineering, v. 28, n. 3, 2021.

Souza, T. A. Z., J. L. J. Pereira, M. B. Francisco, C. A. R. Sotomonte, B. Jun Ma, G. F. Gomes & C. J. R. Coronado (2022) Multi-objective optimization for methane, glycerol, and ethanol steam reforming using lichtenberg algorithm, International Journal of Green Energy

Tamer, A., Zanoni, A., Cocco, A. et al. A numerical study of vibration-induced instrument reading capability degradation in helicopter pilots. CEAS Aeronaut J 12, 427–440 (2021).

Tan, Y., & Zhang, L. (2019). Computational methodologies for optimal sensor placement in structural health monitoring: A review. Structural Health Monitoring, 147592171987757.

Vinet, D. Gamby, Prediction of long-term mechanical behaviour of fibre composites from the observation of micro-buckling appearing during creep compression tests, Composites Science and Technology, Vol. 68, No. 2, pp. 526–536, (2008).

Voicu, Andrei-Daniel, Hadăr, Anton, Vlăsceanu, Daniel and Pastramă, Ştefan-Dan. (2020). SHM Monitoring Methods and Sensors with Applications to Composite Helicopter Blades: A Review. Acta Universitatis Cibiniensis. Technical Series, vol.72, no.1, pp.1-11.

Worden &Friswell (2009) Keith Worden e Michael I Friswell. Modal–vibration-based damage identification. Encyclopedia of Structural Health Monitoring.

Yang C, Lu Z (2017) An interval effective independence method for optimal sensor placement based on non-probabilistic approach. Sci China Technol Sci 60(2):186–198.

Yi TH and Li HN. Methodology developments in sensor placement for health monitoring of civil infrastructures. Int J Distrib Sens N 2012; 8(8): 612726.

Yuen K-V, Kuok S-C (2015) Efficient bayesian sensor placement algorithm for structural identification: a general approach for multi-type sensory systems. Earthq Eng Struct Dyn 44(5):757–774

Zenzen, I. Belaidi, S. Khatir, M.A. Wahab, A damage identification technique for beam-like and truss structures based on FRF and Bat Algorithm, Comptes Rendus Mécanique 346 (12) (2018) 1253–1266.

Zhou, G. D., Yi, T.-H., Xie, M.-X., Li, H.-N., & Xu, J.-H. (2021). Optimal Wireless Sensor Placement in Structural Health Monitoring Emphasizing Information Effectiveness and Network Performance. Journal of Aerospace Engineering, 34(2), 04020112.